ARMY RESEARCH LABORATORY

Burning-Rate Models and Their Successors: A Personal Perspective

by Martin S. Miller

ARL-TR-2996 **June 2003**

NOTICES

Disclaimers

The findings in this report are not to be construed as an official Department of the Army position unless so designated by other authorized documents.

Citation of manufacturer's or trade names does not constitute an official endorsement or approval of the use thereof.

Destroy this report when it is no longer needed. Do not return it to the originator.

Army Research Laboratory
Aberdeen Proving Ground, MD 21005-5066

ARL-TR-2996 **June 2003**

Burning-Rate Models and Their Successors: A Personal Perspective

Martin S. Miller
Weapons and Materials Research Directorate, ARL

REPORT DOCUMENTATION PAGE	Form Approved OMB No. 0704-0188

1. REPORT DATE *(DD-MM-YYYY)*	2. REPORT TYPE	3. DATES COVERED (From - To)
June 2003	Final	1 September 2002–25 March 2003

4. TITLE AND SUBTITLE
Burning-Rate Models and Their Successors: A Personal Perspective

5a. CONTRACT NUMBER

5b. GRANT NUMBER

5c. PROGRAM ELEMENT NUMBER

6. AUTHOR(S)
Martin S. Miller

5d. PROJECT NUMBER
622618.H80

5e. TASK NUMBER

5f. WORK UNIT NUMBER

7. PERFORMING ORGANIZATION NAME(S) AND ADDRESS(ES)
U.S. Army Research Laboratory
ATTN: AMSRL-WM-BD
Aberdeen Proving Ground, MD 21005-5066

8. PERFORMING ORGANIZATION REPORT NUMBER
ARL-TR-2996

9. SPONSORING/MONITORING AGENCY NAME(S) AND ADDRESS(ES)

10. SPONSOR/MONITOR'S ACRONYM(S)

11. SPONSOR/MONITOR'S REPORT NUMBER(S)

12. DISTRIBUTION/AVAILABILITY STATEMENT
Approved for public release; distribution is unlimited.

13. SUPPLEMENTARY NOTES

14. ABSTRACT

The development of models to compute the burning rate of energetic materials has undergone a paradigm shift in the last 15 years from treating the gas-phase reactions as a few global reactions to attempting to describe all of the elementary reactions involved. This shift toward chemical specificity has brought the promise of true predictive capability in such models. Thwarting this promise, however, has been the unattainability of treating the condensed-phase and surface processes with commensurate detail and assurance. In this work, it is shown that limited predictability has recently been achieved by a semi-empirical finesse of the condensed-phase reactions and surface gasification through the agency of a universal pyrolysis law for certain families of propellant ingredients. It is also argued that the long-range prognosis for generalized predictability arising from a first-principles three-phase model lies with developing submodels for the condensed-phase and surface phenomena based on molecular dynamics (MD). However, since a continuum description of the gas-phase processes will always be preferable, the mating of these MD submodels with the continuum gas-phase description will be a non-trivial research issue. To facilitate the coming dialogue between current continuum modelers and future MD modelers, this work describes the conceptual and mathematical basis of the continuum models in considerable detail. It is suggested that the mating of these disparate descriptions might be accomplished by developing simple, idealized continuum submodels whose parameters and assumptions might be justified by the MD submodels. An example of such a continuum submodel is developed for the process of multicomponent evaporation as a surface-gasification mechanism.

15. SUBJECT TERMS
propellant, burning rate, model, molecular dynamics

16. SECURITY CLASSIFICATION OF:			17. LIMITATION OF ABSTRACT	18. NUMBER OF PAGES	19a. NAME OF RESPONSIBLE PERSON
a. REPORT	b. ABSTRACT	c. THIS PAGE			Martin S. Miller
UNCLASSIFIED	UNCLASSIFIED	UNCLASSIFIED	UL	60	19b. TELEPHONE NUMBER (*Include area code*) 410-306-0718

Standard Form 298 (Rev. 8/98)
Prescribed by ANSI Std. Z39.18

Contents

List of Figures

List of Tables

1. Introduction

The capability to calculate the burning rate of propellants from their ingredients has long been recognized as desirable though, until recently, not realizable. Even today, this capability is limited to classes of energetic materials that have been fairly extensively studied experimentally. So far, the goal of computing all the properties of propellants with ingredients that have never actually been synthesized is still beyond our reach. However, considerable progress towards obtaining properties of notional materials such as heats of formation, density, and detonation sensitivity has been made in the last 10 years. Over the same period of time, fledgling ability to compute the burning rate for unstudied formulations within known classes of propellants has emerged.

What is it that makes the burning-rate calculations so difficult? The combustion of energetic materials involves coupling physical and chemical phenomena in the condensed phase, the gas phase, and at the interface between the two. Our greatest knowledge and experience is centered in the gas phase. We now know that many dozens of chemical species reacting by many hundreds of elementary reactions are at play there in concert with the physical processes of molecular diffusion, convection, and thermal conduction. Even by itself, the gas phase presents us with a daunting array of nonlinear phenomena to understand. Fortunately, general scientific progress over the last several decades has armed us with the experimental and theoretical tools to approach this problem in a systematic way. Though many uncertainties remain, the conceptual means, if not always the resources, are available to resolve them. Such is not the case in dealing with the condensed-phase and interfacial processes. In these cases, we truly do not know what we do not know.

It would seem that the best hope for breaking this impasse lies in molecular dynamics (MD) simulation using reactive potentials, but this approach is fairly said to be in its infancy. Thus far, only continuum-mechanics models have been developed to describe the 2- or 3-phase combustion process, and arguments are easily mounted to suggest that one will always want to use a continuum model to describe the gas phase. Yet, I believe that mating these two descriptions will not be a trivial task. Anticipation of the coming need for communication between practitioners of these two approaches is what motivates this discourse. Accordingly, emphasis is placed on the mathematical framework and concepts behind the continuum-mechanics approach, the history of model development, their current status, and unsolved problems.

2. Phenomena

Before approaching the issues surrounding the mathematical modeling of propellant burning rates, one should become familiar with the range of phenomenological behaviors associated with the combustion of propellants and propellant ingredients. Solid propellants are of two basic types: homogeneous and composite. Single- and double-base propellants are examples of homogeneous propellants. Homogeneous propellants are considered to be well mixed on a molecular scale, although this may not be strictly true because of the practical constraints on mixing. Single-base propellant consists almost exclusively of nitrocellulose (NC), which becomes increasingly less soluble in the manufacturing solvents as its nitration level increases above ~13%N, leading to a very viscous liquid during mixing and extrusion. My first experience in measuring burning rates was with 6-in-long strands of M10.* Based on the measurement technique and degree of control over known variables such as pressure, I was expecting a standard error of about 1%. Instead, the standard deviation in measured burning rates using dozens of 1-in-long specimens was as large as 25%. These large deviations arose from inhomogeneities in the propellant material itself due to imperfect mixing of the highly viscous feedstock material. This was a most inauspicious introduction to my new field! Fortunately, this would become the worst case I would ever encounter in my career. Most other homogeneous propellants benefit from the plasticizing properties of nitroglycerin (NG) and burn very reproducibly. However, one always must be aware, particularly with experimental propellants, that manufacturing procedures may influence the combustion properties in unexpected and nonreproducible ways.

Composite propellants comprise a heterogeneous mixture of crystalline oxidizers and polymeric binders. Double-base propellant with crystalline nitroguanidine (NQ) added (M30) is an example. Only in the last 15 years have composite propellants involving cyclotrimethylenetrinitramine (RDX) come into use for guns. The use of such a secondary explosive as a major ingredient in gun propellant required considerable testing to pass safety criteria for use in the field. Composites utilizing RDX, cyclotetramethylenetetranitramine (HMX), and 2,4,6,8,10,12-hexanitrohexaazaisowurtzitane (CL20) coupled with various energetic polymeric binders are currently under active investigation.

The propellant type can have important consequences for modeling the burning rate. In many cases, it is found that the oxidizer particle size strongly influences the burning rate. If this is so, a one-dimensional (1-D) model may not be suitable. On the other hand, observations of burning surfaces of nitramine-composite propellants (*1*) at pressures on the order of 1 MPa indicate that a melt layer exists at the surface. This melt layer provides an opportunity for the solid ingredients to

* Propellant formulations are given in the Appendix.

become intimately mixed prior to gasification, potentially restoring a 1-D character to the combustion phenomena.

Despite their uniform morphology, one cannot necessarily assume that homogeneous propellants burn one-dimensionally. The following description of double-base propellant combustion is enough to give pause to the most intrepid model builder: "It can be observed visually that the burning surface exhibits a wave-like mode of consumption. It appears as if glowing filaments of carbonaceous material periodically move over the surface consuming a thin layer of propellant. Ciné photography of the propellant surface shows that a smooth area on this surface appears to darken and to roughen. This area is then consumed by a wave of combustion which moves across the surface and leaves behind a network of carbon filaments which are blown off the surface by the steady evolution of gas. ... The consumption of the reacting surface layer leaves a smooth surface which subsequently repeats this sequence. It seems probable that the overall, average rate of burning is the result of two components: a steady rate analogous to the burning of a liquid propellant and a surface or condensed phase reactive wave moving laterally across the surface" (*2*). It is clear that any 1-D model of homogeneous or composite propellant combustion is to be understood as an idealization of the phenomena and not as an exact description.

Despite all of the aforementioned complexities, propellants burn, at least on a macroscopic scale, in "parallel layers" (i.e., in a direction normal to the local surface curvature). This is the property that allows for interior-ballistic control of the net gasification rate through intricate and ingenious propellant-grain geometries. It is also the property that gives the model builder some basis for hope. Another source of encouragement is that most propellants burn with a very simple power-law pressure dependence, despite radical changes in the appearance of the visible flame attached to the burning surface. At pressures below ~1 MPa, there is no visible flame above the burning surface of homogeneous and many composite propellants. As the pressure increases, a weak flame appears ≥1 cm distant from the surface. With further pressure increases, the visible flame resides closer and closer to the surface, under steady-state, constant-pressure conditions. At ≥10 MPa, the flame appears attached directly to the surface. In most cases, this evolving flame behavior does not perturb the power-law pressure dependence of the burning rate. The nonluminous zone between the visible flame and the surface is known as the dark zone, which is now known to be a consequence of the relatively slow reduction of NO to N_2 (and slow reactions involving HCN in the case of nitramines). All this suggests that burning-rate control resides in a thin gas layer close to the surface, an inference that further encourages the 1-D idealization.

3. Concepts

To date, there have been no MD models of multiphase combustion. This may change in the distant future; however, a nearer-term prospect is that MD submodels of the condensed-phase and/or interface processes will be developed and that these submodels will be used to supplement

the continuum-mechanics combustion models. Anticipating the need to merge these two viewpoints, we develop in this section the mathematical formulation of the continuum paradigm.

Studying Figure 1 will provide the reader with some appreciation of the range of phenomena that are involved in the combustion of propellants. No model exists which has treated all of the processes suggested in the figure; the list is intended as a conceptual transition from nature to mathematics. Some propellants are known to exhibit a liquid layer at the burning surface and some may not. I shall assume that, in the general case, a 3-phase (solid, liquid, gas) problem must be solved. The photograph in Figure 1 is of an RDX composite propellant (M43) burning in the steady state at a pressure of 1.6 MPa. In this case, the dark zone is clearly defined, and one can see that the idealization of a 1-D semi-infinite solid does not appear to be unreasonable.

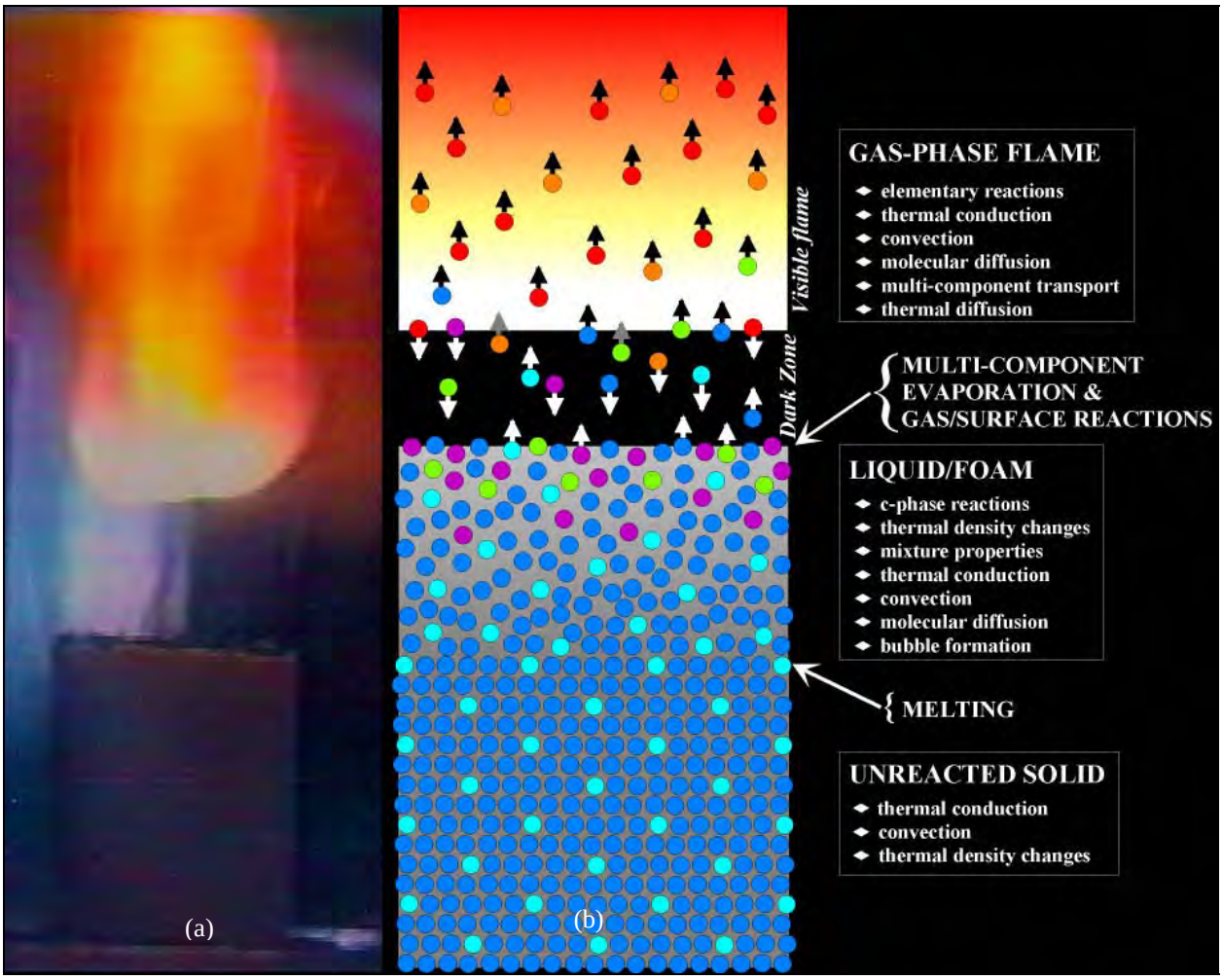

Figure 1. Photograph of an (a) RDX-composite propellant (M43) deflagrating at 1.6 MPa and (b) a caricature of the 3-phase molecular processes involved.

Getting now to the formalism, I consider a semi-infinite solid combusting in the steady state at constant pressure. The spatial coordinate, taken as x, extends from $-\infty$ deep in the solid at an initial temperature of T_0, to the solid/liquid interface at $-x_{liq}$, to the liquid/gas surface at $x = 0$, and finally to the region of equilibrium gas products at the adiabatic flame temperature T_f at $x = \infty$. Equations conserving mass, atomic species, and energy must be solved in each phase subject to the boundary conditions for that phase. The intraphase solutions must also satisfy the equations of continuity at each phase boundary and whatever additional constraints are imposed by the surface-regression mechanism.

3.1 Intraphase Conservation Equations

The conservation equations within each phase are developed and discussed elsewhere (*3*), but will be summarized for convenience and completeness here. The + and – superscripts on the location superscripts indicate the side of the boundary where the values are taken, e.g., $-x_{Liq}^{+}$ means evaluated at the liquid side of the interface at the coordinate $x = -x_{Liq}$.

3.1.1 Solid Phase

Species conservation:

$$\dot{m}\frac{dY_k}{dx} = \dot{\omega}_k W_k \qquad k = 1,2,...,N \quad , \tag{1}$$

assuming molecular diffusion is negligible on a combustion timescale, where $\dot{m}$ is the total mass flux and an eigenvalue for the problem, Y_k is the mass fraction of the kth species, $\dot{\omega}_k$ is the net rate of production of species k due to chemical reactions, W_k is the molecular weight of the kth species, and N is the total number of distinct species in all three phases. These equations are subject to the domain boundary conditions

$$Y_k = Y_k^{-\infty} \qquad k = 1,2,...,N \qquad at \quad x = -\infty . \tag{2}$$

The set of mass fractions $\left\{Y_k^{-\infty}\right\}$ reflect the composition of the unreacted propellant.

Energy conservation:

$$\frac{d}{dx}\left(\lambda_{Sol}\frac{dT}{dx}\right) - \dot{m}\bar{c}_{Sol}\frac{dT}{dx} - \sum_{k=1}^{N_{Sol}}\dot{\omega}_k W_k h_k = 0 . \tag{3}$$

Both the thermal conductivity λ_{Sol} and the average specific heat of the solid mixture $\bar{c}_{Sol}$ are, in general, functions of the independent variable x. W_k is the molecular weight and h_k is the enthalpy of species k. This equation is subject to the domain boundary conditions:

$$T = T_0 \qquad at \quad x = -\infty \tag{4}$$

and

$$T = T_m \qquad at \quad x = -x_{Liq}\,, \tag{5}$$

where T_0 is the initial temperature of the propellant, T_m is the melting point of the propellant compound, and $-x_{Liq}$ is the coordinate of the solid/liquid boundary, which will be an eigenvalue of the complete combustion problem. It should be noted here that these conservation equations for the solid phase and liquid phase in the next section embody precepts deriving from long experience with low-pressure gas-phase processes and may not be as general as presumed. In the gas phase at sufficiently low densities each reaction event takes place in essential isolation. Thermal reaction coefficients, obtained by averaging over velocities and reaction cross sections, can therefore be used to characterize reaction events anywhere and everywhere. In the condensed phase, on the other hand, reactive events do not take place in isolation but in a dielectric field produced by the close proximity of many "spectator" molecules. This dielectric field will evolve as a function of the instantaneous configuration of all the molecules in the vicinity of the reacting molecules during the course of the reaction. The potential therefore exists that there will be too many variables to make the notion of thermal rate coefficients an adequate and useful idealization. Of course, at present the issue is moot in the case of energetic materials as the reactions are virtually unknown. An MD approach, in principle, would handle these complexities in a natural way.

3.1.2 Liquid Phase

All models to date have neglected molecular diffusion in the liquid phase as well, but I retain it in the general formulation here because I later show that it may be of some importance.

Species conservation in liquid phase:

$$\frac{d}{dx}\left(\rho_{Liq} Y_k V_k\right) + \dot{m}\frac{dY_k}{dx} - \dot{\omega}_k W_k = 0 \qquad k = 1,2,...,N \quad , \tag{6}$$

where ρ_{Liq} is the liquid density and V_k is the diffusion velocity of species k. These equations are subject to the boundary conditions:

$$\dot{m} Y_k^{-x_{Liq}^+} + \rho_{Liq} Y_k^{-x_{Liq}^+} V_k^{-x_{Liq}^+} = \dot{m} Y_k^{-x_{Liq}^-} \qquad k = 1,2,...,N \qquad at \quad x = -x_{Liq} \tag{7}$$

and

$$Y_k = Y_k^{0^-} \qquad k = 1,2,...,N \qquad at \quad x = 0\,. \tag{8}$$

Energy conservation in liquid phase:

$$\frac{d}{dx}\left(\lambda_{Liq}\frac{dT}{dx}\right) - \dot{m}\bar{c}_p^{Liq}\frac{dT}{dx} - \sum_k^N \rho_{Liq} Y_k V_k c_p^k - \sum_{k=1}^N \dot{\omega}_k W_k h_k = 0\,, \tag{9}$$

subject to the boundary conditions:

$$T = T_m \qquad at \quad x = -x_{Liq} \tag{10}$$

and

$$T = T_s \qquad at \quad x = 0\,. \tag{11}$$

3.1.3 Gas Phase

Species conservation in gas phase:

$$\frac{d}{dx}\left(\rho_{Gas} Y_k V_k\right) + \dot{m}\frac{dY_k}{dx} - \dot{\omega}_k W_k = 0 \qquad k = 1,2,...,N. \tag{12}$$

subject to the boundary conditions:

$$\dot{m}Y_k^{0^-} + \rho_{Liq} Y_k^{0^-} V_k^{0^-} = \dot{m}Y_k^{0^+} + \rho_{Gas} Y_k^{0^+} V_k^{0^+} \qquad k = 1,2,...,N \qquad at \quad x = 0 \tag{13}$$

and

$$\frac{dY_k}{dx} = 0 \qquad k = 1,2,...,N \qquad at \quad x = \infty. \tag{14}$$

Energy conservation in gas phase:

$$\frac{d}{dx}\left(\lambda_{Gas}\frac{dT}{dx}\right) - \dot{m}\bar{c}_p^{Gas}\frac{dT}{dx} - \sum_k^N \rho_{Gas} Y_k V_k c_p^k - \sum_{k=1}^N \dot{\omega}_k W_k h_k = 0, \tag{15}$$

subject to the boundary conditions:

$$T = T_s \qquad at \quad x = 0 \tag{16}$$

and

$$\frac{dT}{dx} = 0 \qquad at \quad x = \infty. \tag{17}$$

There is, finally, the mass conservation equation

$$\frac{d\dot{m}}{dx} = 0, \tag{18}$$

which has the trivial solution

$$\dot{m} = cons\tan t = \rho_s^0 r, \tag{19}$$

through all three phases. In particular, at T_0, the solid-phase density is ρ_s^0 and the linear burning rate is r.

3.2 Phase-Matching Continuity Conditions

Some of the above boundary conditions are expressed in quantities that are unknown at the outset and coupled to solutions in adjacent domains. These initially unknown quantities, $\dot{m}$, T_s, x_{Liq},

and $\left\{Y_k^{0^-}\right\}$ are the eigenvalues for the complete problem. The final solutions for the temperature and mass fractions in each domain must satisfy the conservation equations with their respective boundary conditions in each phase for unique values of the eigenvalues. In order to accomplish this, one needs further constraints on the problem. These are to be found in the inter-phase equations of continuity, discussed in this section, and in the surface-regression mechanism, discussed in the next section. Figure 2 shows the contributions to the energy fluxes across the phase boundaries. The meaning of the subscripts and superscripts will be clear from the figure contexts. The continuity conditions at each phase interface are constructed by equating the summed contributions on each side of a particular interface. In the figure, I have neglected contributions from the kinetic energy, as these are very small for typical propellant burning rates (of order 0.01% of the starting enthalpies), and also contributions from molecular diffusion in the solid phase, because it will be too slow on the time scale of importance to combustion. The boundary conditions are shown in Figure 2.

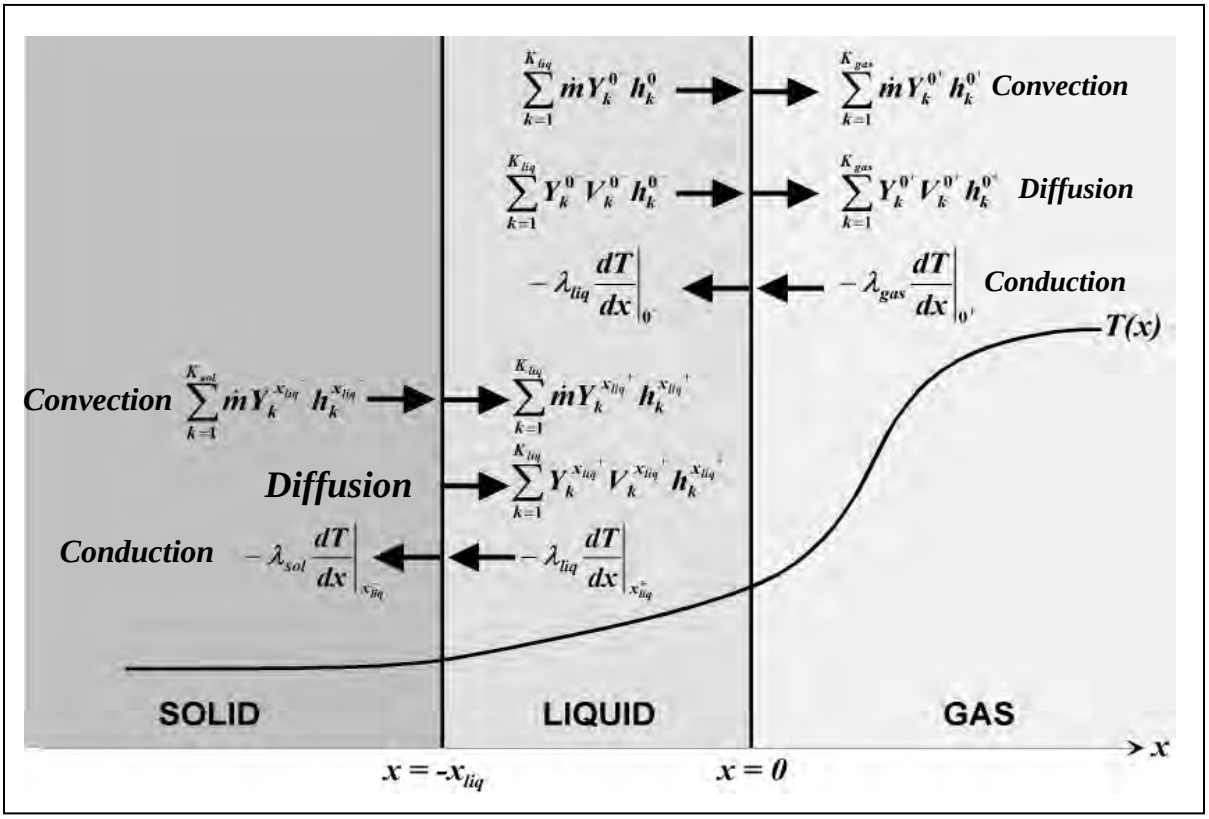

Figure 2. Energy fluxes at the phase boundaries arising from convection, molecular diffusion, and thermal conduction.

3.2.1 Species-Flux Continuity at Solid/Liquid Boundary, $x = -x_{Liq}$

This relation is the same as equation 7 and thus is not a new constraint.

3.2.2 Energy-Flux Continuity at Solid/Liquid Boundary, $x = -x_{Liq}$

$$-\lambda_{Sol}\left(\frac{dT}{dx}\right)^{-x_{Liq}^{-}} + \dot{m}\sum_{k}^{N} Y_k^{-x_{Liq}^{-}} h_k^{-x_{Liq}^{-}} = -\lambda_{Liq}\left(\frac{dT}{dx}\right)^{-x_{Liq}^{+}} + \dot{m}\sum_{k}^{N} Y_k^{-x_{Liq}^{+}} h_k^{-x_{Liq}^{+}} + \rho_{Liq}\sum_{k}^{N} Y_k^{-x_{Liq}^{+}} V_k^{-x_{Liq}^{+}} h_k^{-x_{Liq}^{+}} . \quad (20)$$

3.2.3 Species-Flux Continuity at Liquid/Gas Boundary, $x = 0$

This relation is the same as equation 13 and thus is not a new constraint.

3.2.4 Energy-Flux Continuity at Liquid/Gas Boundary, $x = 0$

$$-\lambda_{Liq}\left(\frac{dT}{dx}\right)^{0^-} + \dot{m}\sum_{k}^{N} Y_k^{0^-} h_k^{0^-} + \rho_{Liq}\sum_{k}^{N} Y_k^{0^-} V_k^{0^-} h_k^{0^-} = -\lambda_{Gas}\left(\frac{dT}{dx}\right)^{0^+} + \dot{m}\sum_{k}^{N} Y_k^{0^+} h_k^{0^+} + \rho_{Gas}\sum_{k}^{N} Y_k^{0^+} V_k^{0^+} h_k^{0^+} . \quad (21)$$

3.3 Surface Regression Mechanism

In general, one might consider that many mechanisms contribute to surface regression during combustion: evaporation or desorption of surface species without change of identity, reaction of surface species to produce different gas-phase species, reaction of gas-phase species with surface species to produce other gas-phase species, and, possibly, physical ejection of molecular aggregates due to explosive reaction in the surface. It is also possible that some combination of these mechanisms might be active in the condensed phase below the surface, creating bubbles which are subsequently convected to the surface and released. Obviously, it will be a very great challenge to include all of these processes in a full combustion model, although attempts have been made to model RDX using a mix of evaporation and bubble formation (*4*, *5*). In these treatments, one-dimensionality was preserved through the artifice of continuous porosity, though with unknown accuracy. In my opinion, the only surface-regression mechanism that has been treated with reasonable rigor is evaporation, and even this has been approximate with unknown accuracy. The remainder of this section will be devoted to a discussion of the approach taken to an evaporative mechanism and its potential shortcomings.

3.3.1 Single-Component Evaporation Mechanism

To date, the only evaporation mechanism used in published burning-rate model developments is based on the following reasoning. Consider a pure liquid substance in equilibrium with its vapor at some temperature T_s. I will refer to the multiphase presence of a single chemical species as "single component." At equilibrium, the mass flux impinging on the surface is given by the kinetic-theory result $\frac{1}{4} n\bar{v} W$, where n is the molar number density in the vapor, $\bar{v}$ is the mean molecular velocity at T_s, and W is the molecular weight of the species being considered. If α is the fraction of impinging molecules that are absorbed into the surface (i.e., the accommodation coefficient), then the mass flux actually absorbed into the surface is $\frac{1}{4}\alpha n\bar{v} W$. Under equilibrium conditions, the mass flux escaping the surface equals the mass flux being absorbed. Thus, the escaping mass flux

can be expressed in terms of the number density at equilibrium or, through the equation of state, the equilibrium vapor pressure p^e. Under combustion conditions, the vapor pressure at the surface is less than the equilibrium value due to depletion by reactions and molecular diffusion. Thus, one can express the net regression rate of the surface during combustion in terms of the equilibrium vapor pressure at T_s, the total pressure, and the mole fraction of the mother-liquor species on the gas-phase side of the surface, X^{0^+}. These arguments are summarized graphically in Figure 3 and in equation 22, which expresses the net flux of evaporating molecules as the difference between the gross escaping flux and the gross condensing flux, i.e.,

$$\dot{m}\left(X^{0^+}, T_s\right) = \alpha\left(\frac{W}{2\pi R T_s}\right)^{\frac{1}{2}}\left[p^e\left(T_s\right) - X^{0^+} p_{total}\right] \quad . \tag{22}$$

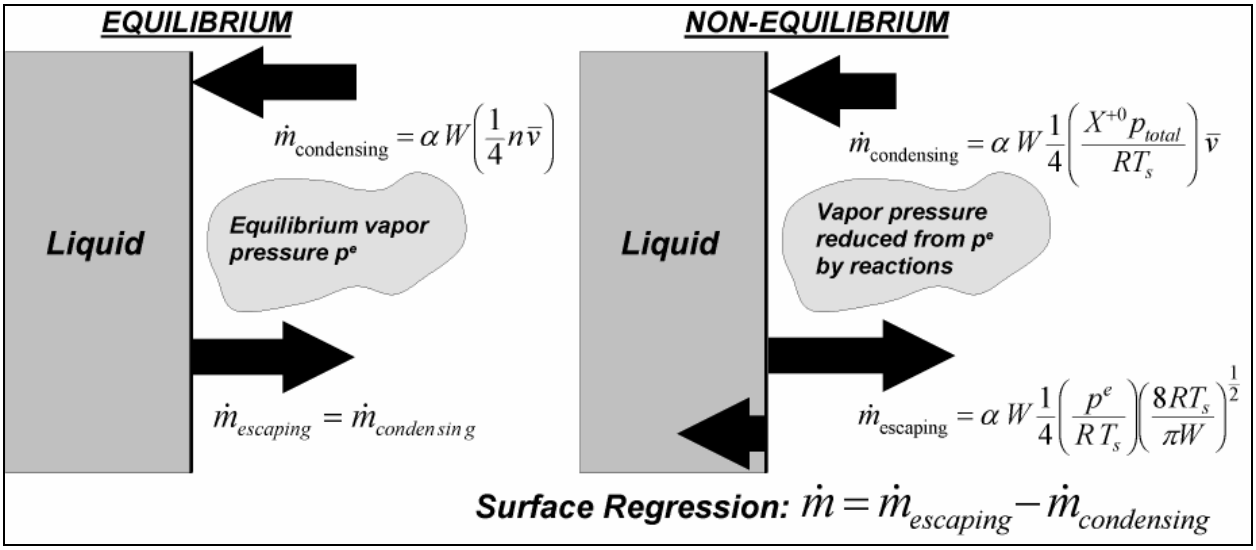

Figure 3. Single-component evaporative surface-regression mechanism.

3.3.2 Multicomponent Evaporation Mechanism

On the face of it, there is no problem with the rigor of the arguments just presented. The difficulty comes when applying it to even the simplest combustion problem. Take the self-deflagration of pure frozen ozone, for instance. This case will be developed more fully later, but it serves to illustrate the problem with single-component evaporation. Under combustion conditions, by definition, there will be chemical species other than ozone in the gas phase. These will be products and intermediates of ozone decomposition, i.e., O_2 and O. These other species will also impinge upon and be absorbed to some extent in the surface. Thus, the surface will have a multicomponent nature, and the equilibrium vapor pressure of pure ozone will no longer determine the mass flux of ozone escaping the surface but also be a function of the mole fractions and molecular properties of the other molecules present. In addition, the mass flux leaving the surface will include contributions from the surface-absorbed products and intermediates originating from the gas-phase

reactions. In principle, then, the single-component evaporation mechanism is intrinsically inappropriate for a problem involving combustion. Of course, as an approximation, it may turn out to be useful, but its accuracy is impossible to assess a priori.

3.4 Mathematical Closure of the 3-Phase Problem

To illustrate the final posing of the 3-phase mathematical problem, I adopt single-component evaporation as the surface-regression mechanism and assume that molecular diffusion in the liquid phase can be neglected. Neglect of molecular diffusion means that only one boundary condition in the liquid-phase domain is required and I choose this to be

$$Y_k = Y_k^{-x_{Liq}} \qquad k = 1,2,...,N \qquad at \quad x = -x_{Liq}\,. \tag{23}$$

Note that in the absence of diffusion, $Y_k^{-x_{Liq}^-} = Y_k^{-x_{Liq}^+}$. This single boundary condition replaces equations 7 and 8. Neglect of diffusion, through replacement of equation 8, also greatly simplifies the problem by reducing the number of eigenvalues to three, x_{Liq}, T_s, and $\dot{m}$. One begins by providing starting estimates for these three eigenvalues of the coupled boundary-value problems; call them $\hat{x}_{Liq}$, $\hat{T}_s$, and $\hat{\dot{m}}$. The solid phase conservation equations are then solved using the estimated values $\hat{x}_{Liq}$ and $\hat{\dot{m}}$. This solution will provide values of $\left\{Y_k^{-x_{Liq}}\right\}$ needed by the liquid-phase boundary condition equation 23. After solving the liquid-phase conservation equations test to see if

$$\lambda_{Sol}\left(\frac{dT}{dx}\right)_{x=-\hat{x}_{Liq}} \stackrel{?}{=} \lambda_{Liq}\left(\frac{dT}{dx}\right)_{x=-\hat{x}_{Liq}} + \dot{m}\sum_k^N Y_k^{-\hat{x}_{Liq}}\left[h_k^{Liq}(T_m) - h_k^{Sol}(T_m)\right]. \tag{24}$$

This is equation 20 rewritten for the neglect of liquid-phase diffusion. The quantity in brackets is the latent heat of fusion for simple substances. If the equality is not met at some chosen level of approximation, then choose another value of x_{Liq} and repeat until equation 24 is satisfied. When equation 24 is satisfied, solve the gas-phase conservation equations using the liquid-phase solutions just obtained for $\left\{Y_k^{0^-}\right\}$, then test to see if the surface regression mechanism is satisfied, i.e., if

$$\hat{\dot{m}}\left(X^{0^+}, \hat{T}_s\right) \stackrel{?}{=} \alpha\left(\frac{W}{2\pi R\hat{T}_s}\right)^{\frac{1}{2}}\left[p^e\left(\hat{T}_s\right) - X^{0^+}\,p_{total}\right]. \tag{25}$$

Normally, equation 25 will not be satisfied at this point. Choose another value of $\hat{\dot{m}}$ and solve the solid, liquid, and gas phases again, iterating until both equations 24 and 25 are satisfied. Then test to see if

$$-\lambda_{Liq}\left(\frac{dT}{dx}\right)^{0^-} \stackrel{?}{=} -\lambda_{Gas}\left(\frac{dT}{dx}\right)^{0^+} + \hat{\dot{m}}\sum_k^N\left(Y_k^{0^+}h_k^{0^+} - Y_k^{0^-}h_k^{0^-}\right) + \rho_{Gas}\sum_k^N Y_k^{0^+}V_k^{0^+}h_k^{0^+}\,. \tag{26}$$

This is equation 21 rewritten for the neglect of liquid-phase diffusion. Normally, equation 26 will not be satisfied at this point, so choose another value of $\hat{T}_s$ and iterate all of the above until equations 24–26 are all satisfied to the required degree of accuracy. At this point, one will have determined the eigenvalues of the problem, x_{Liq}, T_s, and $\dot{m}$. The whole process can be more easily visualized as a logic flow chart in Figure 4. Actually, the process is straightforward and successive guesses for the eigenvalues can be based on physical reasoning depending on the results of each energy-flux equality test so that convergence of each eigenvalue can be approached with monotonic decreasing error. The solution process is obviously more complicated if molecular diffusion in the liquid phase is not neglected.

4. Models

The quantitative modeling of the burning rate of solid energetic materials really began in the dark hours of World War II with, predominantly, the efforts of Parr and Crawford (*6*) at the University of Minnesota and Rice and Ginell (*7*) at the University of North Carolina. These and related wartime works were published in a special issue of the (then) *Journal of Physical and Colloid Chemistry*. At that time, virtually all propellants, gun and rocket, used some combination of NC and NG as their energetic ingredient. Since that time, composite propellants consisting of ammonium perchlorate in rubber binders (e.g., in the space shuttle boosters) have dominated the solid rocket propellant applications with solid composites based on HMX in polymeric binders also in use. Fielded gun propellants are still dominated by nitrate-ester propellants although composites of these conventional propellants with NQ are common. The variety of propellant ingredients exacerbates the difficulties faced by combustion modelers both because of their different mechanisms and because of the paucity of detailed experimental data available for many of them. Recent trends are toward even more rapid proliferation of new chemical ingredients such as oxetanes, with their functional-group tailorability, and azides, with their attractive environmental advantages. In addition to enhanced performance and safety, the new constraints of minimal environmental impact in manufacture, use, and demilitarization are now driving concerns in the development of new propellants. Coincident with the emergence of many promising new energetic materials, with attendant dilution of experimental characterization, is the growing urgency for theoretical guidance in the formulation of propellants incorporating these materials. It is generally true that the higher the performance required of the weapon system, the smaller the margin of safety will be in the functioning of all the components of the system including the propellant. If having a burning-rate model was deemed important 50 years ago, it is considerably more so with today's new mix of developmental constraints and advanced ingredients.

In this section, my aim is not to give a comprehensive history of burning-rate modeling but, rather, to provide a sense of the conceptual development of modeling approaches. This background is

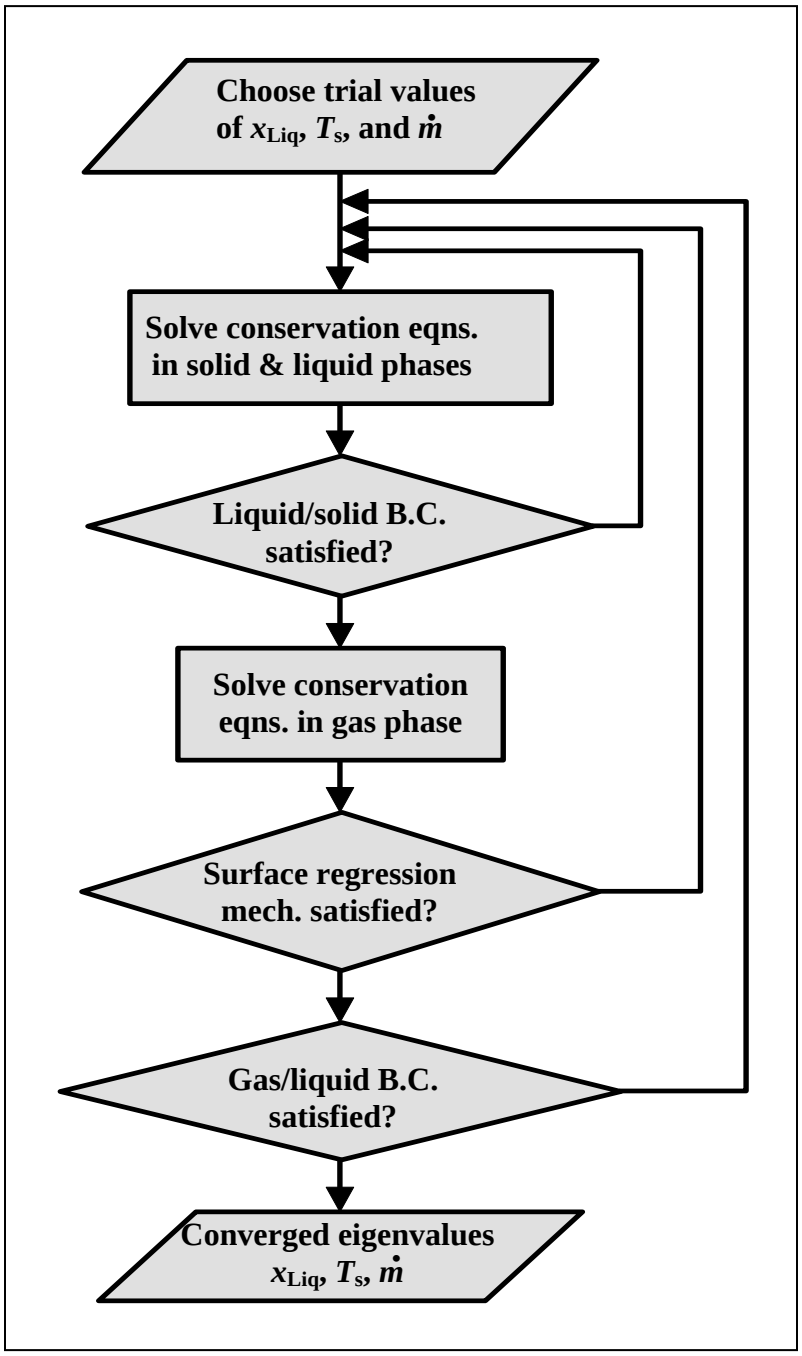

Figure 4. Flow chart illustrating the logic for determining the eigenvalues for the 3-phase problem for single-component evaporation.

essential to an assessment of future avenues of progress in the field. Three subtopics will be addressed: frozen ozone, RDX, and multi-ingredient propellants. This progression of increasing system complexity allows us to illustrate some of the detailed mechanistic challenges facing the model builder and some new approaches to realizing a workable tool for the propellant formulator.

4.1 Frozen Ozone

Frozen ozone is the simplest chemical system falling within the scope of 3-phase self-sustained deflagration. Though simple from a theoretical point of view, it is anything but a straightforward subject for experimental investigation. Its propensity to detonate is legendary and the attendant dangers have undoubtedly inhibited the kind of extensive measurements of burning rate that one would like for comparison with model outputs. On the other hand, a wealth of high-quality experimental data has been obtained on thermophysical properties such as specific heat, thermal conductivity, melting and boiling points, latent heats, reaction paths and rates, and equations of state. This comprehensiveness and reliability of the input database on frozen ozone, coupled with its simplicity, makes it an attractive subject for modeling despite the paucity of burning-rate data. Its conceptual simplicity encourages and enables a more thorough study of mechanisms than with any other energetic material.

Frozen ozone melts at about 80 K and has a normal boiling point of 161.3 K. The rate of reaction in the condensed phase is known to be very slow compared to the time scale of self-sustained deflagration. Thus, all of the uncertainties of describing condensed-phase reactions are conveniently (and legitimately!) sidestepped. The gas-phase reaction mechanism is known with good confidence to consist of the following three reactions:

$$O_3 + M \leftrightarrow O_2 + O + M \qquad \Delta H^0_{298.15K} = +25.65\ kcal/mol\ ; \qquad \text{(I)}$$

$$O_3 + O \leftrightarrow O_2 + O_2 \qquad \Delta H^0_{298.15K} = -93.41\ kcal/mol\ ; \qquad \text{(II)}$$

$$O + O + M \leftrightarrow O_2 + M \qquad \Delta H^0_{298.15K} = -119.06\ kcal/mol\ . \qquad \text{(III)}$$

If one is considering a pure ozone feedstock, then equation 22 describes the mass flux resulting from evaporation. The only measurement of the linear deflagration rate of condensed-phase ozone was made by Streng (*8*) for a liquid mixture of 90% O_3 with 10% O_2. The total mass flux leaving the surface in this multicomponent case is

$$\dot{m} = \dot{m}\left(1 - Y_{O_3}^{0^-}\right) + \dot{m}_{O_3}\,, \qquad (27)$$

an equation first used by Ben-Reuven and Caveny (*9*) in connection with an RDX evaporation model. $\dot{m}_{O_3}$ is the mass flux of O_3 alone. Assuming that $Y_{O_3}^{0^-} \approx Y_{O_3}^{-\infty}$ (i.e., no liquid-phase reactions or molecular diffusion), this expression reduces to

$$\dot{m} \approx \frac{\dot{m}_{O_3}}{Y_{O_3}^{-\infty}} \quad . \qquad (28)$$

This mass-fraction-equivalency assumption is not strictly true for a number of reasons to be discussed subsequently, but it may be an adequate approximation. $\dot{m}_{O_3}$ may be computed using a modification of equation 22 in which the equilibrium vapor pressure term p^e is replaced by the O_3

partial pressure, which may be approximated by $X_{O_3}^{0^-} p_{O_3}^e$, an expression of Raoult's law for ideal solutions. $X_{O_3}^{0^-}$ is the O_3 mole fraction at the surface, which is assumed to be approximated by $X_{O_3}^{-\infty}$, consistent with equation 28. Of course, Raoult's law is only an approximation that can sometimes result in considerable error.

An example of a calculation (*10*) of the burning rate of *pure* frozen ozone at 0.1 MPa and initial temperature 40 K is given in Figure 5. As indicated in the figure, the computed linear burning rate is 0.25 cm/s at 0.1 MPa and an initial temperature of 40 K. By comparison, pure RDX burns ~1 order of magnitude more slowly at a sevenfold higher initial temperature! It is interesting that the surface temperature is ~3 K lower than the boiling point at this pressure. An earlier model (*11*) assumed that the surface temperature is equal to the boiling point; evidently, in this case, it is not a bad assumption. Unlike any of the burning-rate calculations for more complex systems, such as RDX, the calculations by Miller (*10*) include the effects of thermal diffusion in the gas phase, although the burning rate is changed by only a few percent if this process is neglected.

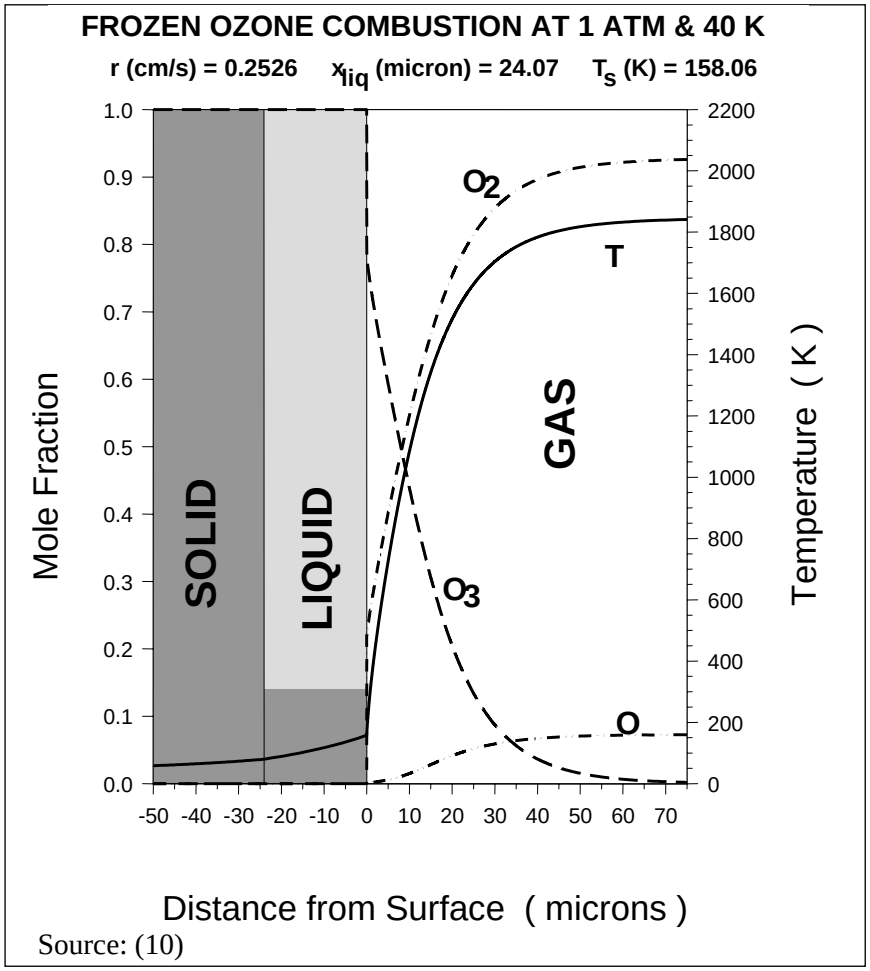

Source: (10)

Figure 5. Computed eigenvalues and profiles for the steady-state deflagration of frozen ozone at 0.1 MPa and an initial temperature of 40 K.

Another mechanism investigated by Miller (*10*) and unique to this ozone study, is the possibility of a heterogeneous reaction in which an oxygen atom from the gas phase reacts with a surface ozone molecule resulting in two gas-phase O_2 molecules:

$$O(gas) + O_3(liq) \rightarrow 2\ O_2(gas) \qquad \Delta H^0_{298.15K} = -93.41\ kcal/mol\ . \qquad (IV)$$

This reaction apparently has never been measured but seems not only plausible but probable. It was assumed that the probability is unity in order to determine the maximum effect. Surprisingly, the burning rate increased only 1% at 0.1 and 2.0 MPa, despite this highly exothermic reaction occurring at the surface, where it adds directly to the heat feedback. In addition to the enhanced heat feedback, this reaction contributes to the destruction of ozone on the surface and should thereby contribute directly to the regression rate. It turns out that the O atoms near the surface that are consumed by the heterogeneous reaction would be consumed anyway in the reaction zone between 1 and 10 μm from the surface in the gas phase, and reactions this close to the surface contribute their heat with high efficiency to the heat feedback (Figure 6). The analysis leading to this conclusion is based on an important concept in steady-state combustion that can be gained from a study of the previously mentioned conservation equations. Starting with equation 15 and assuming that the mixture thermal conductivity is constant and that the specific heats for all species are equal and constant, one can show (*12*) that

$$\lambda_{Gas}\left(\frac{dT}{dx}\right)_{x=0^+} = \int_0^\infty q(x)e^{-\frac{\dot{m}\bar{c}_p}{\lambda_{Gas}}x}\,dx\,, \qquad (29)$$

where *q(x)* is the net volumetric rate of heat release in the gas phase. This expression indicates that heat released within a characteristic transport distance, $\frac{\lambda_{Gas}}{\dot{m}\bar{c}_p}$, will contribute to the heat feedback with high efficiency. Equation 29 is valuable in very complex reaction mechanisms to sort out which reactions are materially affecting the burning rate. The characteristic distance is ~10 μm in Figures 5 and 6.

The ozone problem is simple enough to achieve a complete and unambiguous analysis of the chemistry in each part of the flame. The monotonic behavior of the temperature profile in Figure 5 belies the underlying complexity of parallel and sequential reactions, which switch directions during the course of the flame, as seen in Figure 6. A curiosity indicated in Figure 6 is that *spatially* the first reaction step in the *ozone decomposition flame* is the *production of ozone* by reaction I running in reverse. In more complex reaction mechanisms with dozens of species and hundreds of reactions, it is impossible to completely analyze the chemistry. In those cases sorting tools such PREAD (*13*), ChemPlot (*14*), and ELEMAP (*15*) coupled with considerable experience are essential to gain insights into the mechanisms affecting both the burning rate and the flame features such as the dark zone.

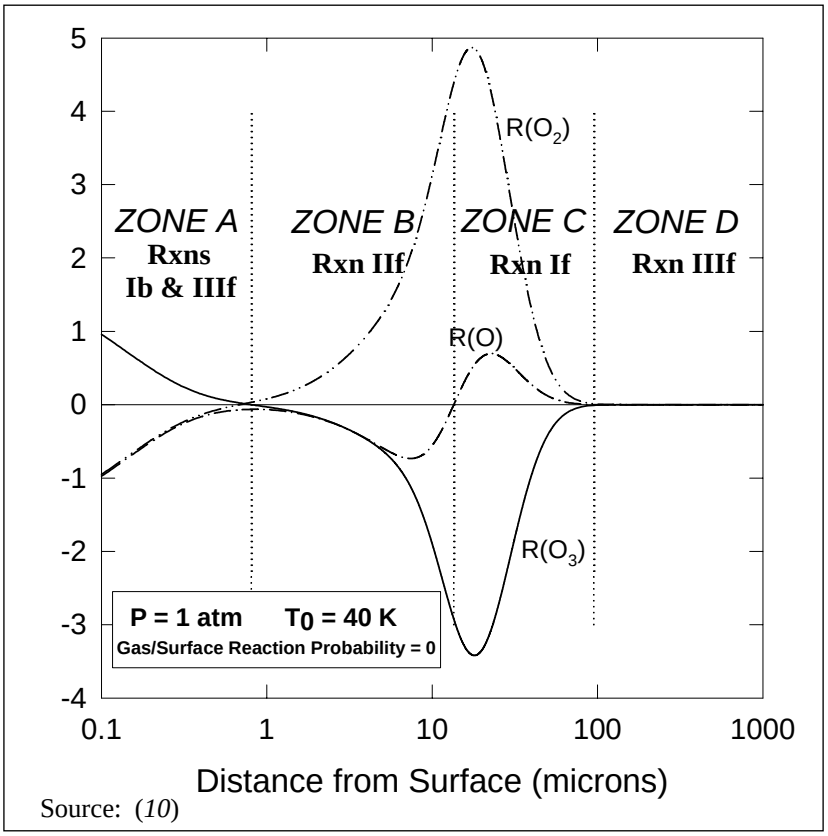

Source: (*10*)

Figure 6. Rates of production of each species in a pure frozen-ozone problem source at 0.1 MPa and 40 K initial temperature. The f and b suffixes indicate that the reaction identified is predominately proceeding in the forward and backward directions, respectively. The whole flame is divided into zones based on the predominant reactions there.

The lone measurement of a condensed-phase burning rate involving ozone, to which I previously alluded, was for a liquid mixture of 90% O_3 and 10% O_2. The result was ~0.4 cm/s; our calculation, utilizing equation 28 and Raoult's law, produced 0.30 cm/s. Sandri (*11*) has speculated that Streng's measured rate is too high because of heating of the liquid by the flame via conduction through the containing-vessel walls and by radiation from the flame. Plausible as they might be, however, the degree to which errors from these sources affected the burning-rate measurement is not possible to determine. Thus, there may remain a significant error in our burning-rate model, and it is worthwhile to look for shortcomings in the idealization which might account for the discrepancy. If such shortcomings matter to the ozone case, they may well matter in more complex systems as well.

4.2 Deficiencies in the Idealization

4.2.1 Multicomponent Evaporation

As pointed out in section 3.3.2, any combustion problem driven by an evaporative surface-regression mechanism is multicomponent in essence since product species will coexist in the liquid

surface either as a result of the presence of more than one ingredient, condensed-phase reaction or molecular diffusion of gas-phase reaction products back to and adsorption onto the surface. This issue is most easily discussed within the context of the O_3/O_2 mixture problem. Let us assume that there will be no atomic oxygen in the liquid surface due to its high reactivity. The attractive intermolecular forces dominate the heats of vaporization, and the strength of that interaction is ordered as follows: O_3-O_3 > O_3-O_2 > O_2-O_2. The heat of vaporization of an O_3 molecule from a surface of both O_3 and O_2 molecules will therefore be less than that from a surface of pure O_3 because the latent heat is just a measure of the work required to remove an O_3 from the surface. On the other hand, the heat of vaporization of an O_2 molecule from the same surface mixture will be greater than that for O_2 from a pure O_2 surface. These modifications, in turn, alter the equilibrium partial pressures of both O_3 and O_2 outside the mixture surface, and the equilibrium vapor pressure is a key determinant of the surface-regression rate by equation 22. Thus, O_3 will escape at a faster rate and O_2 at a slower rate from a surface mixture of the two substances than would be expected using the single-component evaporation formulation coupled with equation 28.

Beyond the greater difficulty of computing the rates of escape of each of the molecules in a multi-component description, there are now fundamental consequences to the posing of the mathematical problem. Though the mass fluxes of O_3 and O_2 leaving the surface are different, in order to maintain a steady state, the linear rates of regression of both species must be equal, i.e.,

$$r_{O_3} = r_{O_2} . \tag{30}$$

Since

$$\dot{m}_{O_3} = Y_{O_3}^{0^-} \rho r_{O_3} \tag{31}$$

and

$$\dot{m}_{O_2} = Y_{O_2}^{0^-} \rho r_{O_2} , \tag{32}$$

then

$$\frac{\dot{m}_{O_3}}{Y_{O_3}^{0^-}} = \frac{\dot{m}_{O_2}}{Y_{O_2}^{0^-}}. \tag{33}$$

I have assumed that the liquid surface is composed only of O_3 and O_2. This means that

$$Y_{O_2}^{0^-} = 1 - Y_{O_3}^{0^-} ; \tag{34}$$

$\dot{m}_{O_3}$ and $\dot{m}_{O_2}$ can be obtained from equation 22, modified as previously described, using the proper multicomponent equilibrium partial pressures for each species, of course. Ideally, one would also dispense with Raoult's law by computing the partial pressures based, for example, on model potential-energy functions as described in section 5.1. However, I am now left with a new

unknown or eigenvalue of the problem, $Y_{O_3}^{0^-}$, with equation 33 as a new constraint. I now must add a new nested loop to the flow chart in Figure 4. While this is a serious increase in computational complexity for the ozone problem, it becomes an overwhelming increase in complexity for a compound like RDX which has dozens of potential species in the surface. Taking the general case where there are *n* chemical species in the surface, the number of eigenvalues, and hence nested loops, will be (*n* + 2). Solution of a complex set of equations like this may be possible, but it will undoubtedly require a different approach than nested loops, possibly a global optimization scheme in which trial values of all of the variables are changed after each iteration.

4.2.2 Liquid-Phase Diffusion

In the O_3/O_2 mixture case, the inclusion of multicomponent evaporation will mean that the mass fractions of O_3 and O_2 at the liquid side of the surface are different from the proportions in the feedstock at $-\infty$. This is illustrated in Figure 7. Since there are no reactions in the liquid phase (by justifiable assumption) the discontinuity in feedstock/surface mass fractions will be resolved in nature by molecular diffusion, which must be considered as an attendant consequence of treating multicomponent evaporation. Because diffusion is generally slow in liquids, it will manifest itself in this case as very steep gradients in the species just below the surface. Obviously, a whole new class of supportive data will be required.

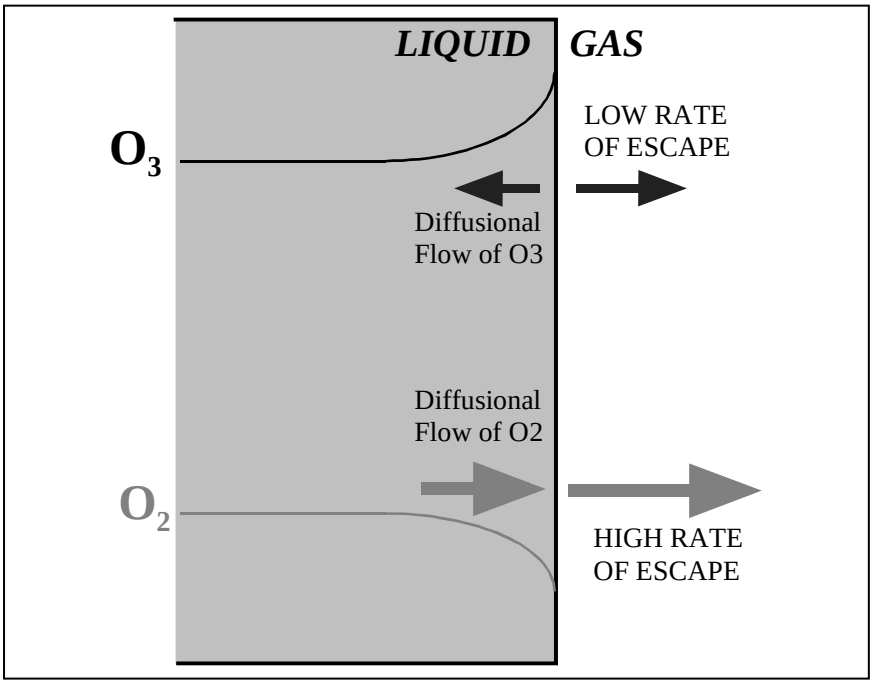

Figure 7. Muticomponent mixture of O_3 and O_2 illustrating how the differing rates of evaporation of the two components result in depletion of O_2 mole fraction and enrichment of the O_3 mole fraction at the surface necessitating the consideration of liquid-phase molecular diffusion to ensure species continuity.

4.2.3 Real-Gas Equation of State

Since our calculations of the burning rate of frozen ozone and the liquid O_3/O_2 mixtures assumed an ideal-gas equation of state, it is worth considering if real-gas effects play a role. The critical pressure and temperature of ozone are 5.46 MPa and 261.1 K, so the shortfall in computed burning rate at 0.1 MPa cannot be attributed to this source. However, calculations by Miller (*10*) for frozen ozone were performed for pressures up to 2 MPa. At 2 MPa and 40 K initial temperature, the computed surface temperature is 217 K. Using standard tables (*16*), one finds that ozone gas at the surface has a compressibility factor ($\frac{pv}{RT}$, where v is the molar volume) of about 0.75. At these conditions, the attractive molecular forces are dominating and number densities are higher than ideal, speeding up the reactions. At the same time, for pressures near the critical point, the heat of vaporization is decreasing rapidly; this means that a given amount of heat feedback will vaporize more surface molecules. Thus, it is possible that use of a real-gas equation of state could have significant impact on a burning-rate calculation. To our knowledge, there are no published burning-rate calculations using a real-gas equation of state.

4.2.4 Phase Separation

Below ~93 K, mixtures of O_3 and O_2 separate into two phases, the upper one being O_2 rich and the lower one O_3 rich. The proportion in each phase depends on the temperature. At the boiling point of liquid O_2, 90.2 K, for example, a starting mixture of 50% O_3 by weight, O_3 in the upper layer ultimately settles to 12% by weight and 38% by weight in the lower phase. Streng's measurement of the burning rate of a 90% O_3/10% O_2 mixture was conducted in a 9-mm Pyrex* tube cooled on the outside by liquid oxygen. No mention is made of the presence of two phases during combustion of the mixture, but if the temperature were actually 90.2 K, two liquid phases may have been present. It is possible that this phenomenon could explain the discrepancy between his measured rate and our computed one, since the O_2-rich upper layer might be expected to evaporate faster. On the other hand, this would lead to a progressively richer mixture as the O_2 selectively escaped; in turn, the specimen would not burn at a steady rate. It also might have been the case that the mixture surface regressed too fast to establish this phase separation. Finally, the presence of the flame inside the tube may have warmed the liquid mixture a few Kelvins, reaching the point where O_3 and O_2 are miscible in all proportions.

4.3 RDX

By far, the most intensive efforts to compute burning rate based on elementary gas-phase reactions have been directed towards neat RDX. It is known that RDX chemically decomposes both in the solid and liquid phases, but the solid-phase reaction is slow and probably not relevant to combustion time scales (*17*). RDX also has a relatively high vapor pressure and was hypothesized to gasify during steady combustion by evaporation first by Ben-Reuven and Caveny (*9*), whose

* Pyrex is a registered trademark of Corning Inc.

model employed global reactions in the gas phase. The first use of the evaporation mechanism in a model with elementary gas-phase reactions was by Melius (*18*) ,who also assumed the single condensed-phase reaction,

$$\text{RDX(Liq)} \rightarrow 3\ CH_2O + 3\ N_2O. \qquad \text{(V)}$$

His calculated burning rates at 0.1 and 2 MPa are in excellent agreement with experimental data.

Other elementary gas-phase reaction RDX models combining evaporation and liquid-phase reactions include those of Liau and Yang (*4*), Davidson and Beckstead (*5*), and Prasad et al. (*19*). The last of these works, though sharing most of the same condensed- and gas-phase reactions as the first two, is a semi-empirical model, requiring the experimental value of the surface temperature to obtain the burning rate, and will not be discussed here. Both Liau and Yang and Davidson and Beckstead assume that reaction V occurs and one other liquid-phase RDX decomposition reaction. In the Liau and Yang model, this other reaction is

$$\text{RDX(Liq)} \rightarrow 3\ HCN + 3/2\ NO + 3/2\ NO_2 + 3/2\ H_2O, \qquad \text{(VI)}$$

whereas in the Davidson and Beckstead model, it is

$$\text{RDX(Liq)} \rightarrow 3\ H_2CN + 3\ NO_2. \qquad \text{(VII)}$$

Both models assume that RDX can form bubbles in the liquid layer and that the following secondary reaction takes place in the bubbles:

$$NO_2 + CH_2O \rightarrow NO + CO + H_2O. \qquad \text{(VIII)}$$

The reaction parameters chosen by each of the authors are given in Table 1.

Both models describe the melt region as 2-phase, consisting of liquid and bubbles; however, since both models are 1-D, this 2-phase character is treated in the conservation equations as a continuous "porosity," ϕ, defined as the ratio of the cross-sectional area occupied by the gas to the total cross-sectional area. The rate of evaporation into "bubbles," or more accurately, into the porosity, is computed using equation 22 at the local subsurface temperature instead of the surface temperature and the "surface area" of bubbles defined by Liau and Yang (*4*) as

$$\begin{aligned} A_{bubbles} &= (36\pi n)^{1/3}\phi^{2/3} \quad , \quad \phi < \frac{1}{2} \\ A_{bubbles} &= (36\pi n)^{1/3}(1-\phi)^{2/3} \quad , \quad \phi > \frac{1}{2}\,. \end{aligned} \qquad \text{(35)}$$

where n is the bubble number density. These equations were given without explanation, except to say that n was to be determined empirically. Davidson and Beckstead (*5*), who used these same equations, evidently understood that n would be a constant, independent of pressure, and they chose 1×10 (*13*) as the appropriate value without further explanation. Liau and Yang provide no value for n used in their calculations.

Table 1. Condensed-phase reaction-rate coefficient parameters assumed by different models for RDX in the Arrhenius form.

Reaction		V	VI	VII	VIII
Melius (*18*)	*A*	4.66×10^{18}	—	—	—
	B	0	—	—	—
	E	47.8 kcal/mol	—	—	—
Liau and Yang (*4*)	*A*	6.0×10^{13}	—	1.6×10^{17}	802
	B	0	—	0	2.77
	E	36 kcal/mol	—	45 kcal/mol	13.73 kcal/mol
Davidson and Beckstead (*5*)	*A*	4.88×10^{11}	6.5×10^{14}	—	802
	B	0	0	—	2.77
	E	36 kcal/mol	45 kcal/mol	—	13.73 kcal/mol

Notes:
Burning-rate calculations based on these models are given in Figure 8.
The Miller (*10*) 3-phase model, assuming no condensed-phase reactions, is applied to RDX, and its results are also shown in Figure 8.
A is in appropriate centimeter, mole, Kelvin, and seconds units.

The consequences of these varied assumptions and data on the computed burning rate are shown in Figure 8. For comparison, I applied our 3-phase code used in the ozone case (*10*) to RDX using the same input data and reaction mechanism employed by Liau and Yang with the exception that no condensed-phase reactions were considered. This model thus assumes that surface regression is by evaporation at the surface only, driven by the heat feedback from reactions in the gas phase whereas in the Liau and Yang model some RDX decomposes in the condensed phase and some RDX evaporates into the liquid-phase porosity (representing bubbles). The close agreement between all of these models and the experimental burning rates (*20–26*) is nothing short of astonishing. Given the varied inputs and assumptions, one is tempted to conclude that the single common element is the evaporative mechanism and that the condensed-phase reactions are not playing a significant role in the burning rate. However, Davidson and Beckstead use a substantially lower vapor pressure (vapor over solid) than that used by Liau and Yang (vapor over liquid) and find a low sensitivity of the burning rate to vapor pressure. Moreover, Davidson and Beckstead predict a fairly large amount of the RDX decomposes in the liquid state, unlike Liau and Yang (Table 2). Unfortunately, Melius did not report the vapor-pressure expression used in his model, and his results are not otherwise directly comparable to the other models because his model used an earlier gas-phase reaction mechanism. All the other models used a mechanism developed by Yetter et al. (*27*) based on Melius's (*18*) but extended with new reactions thought important.

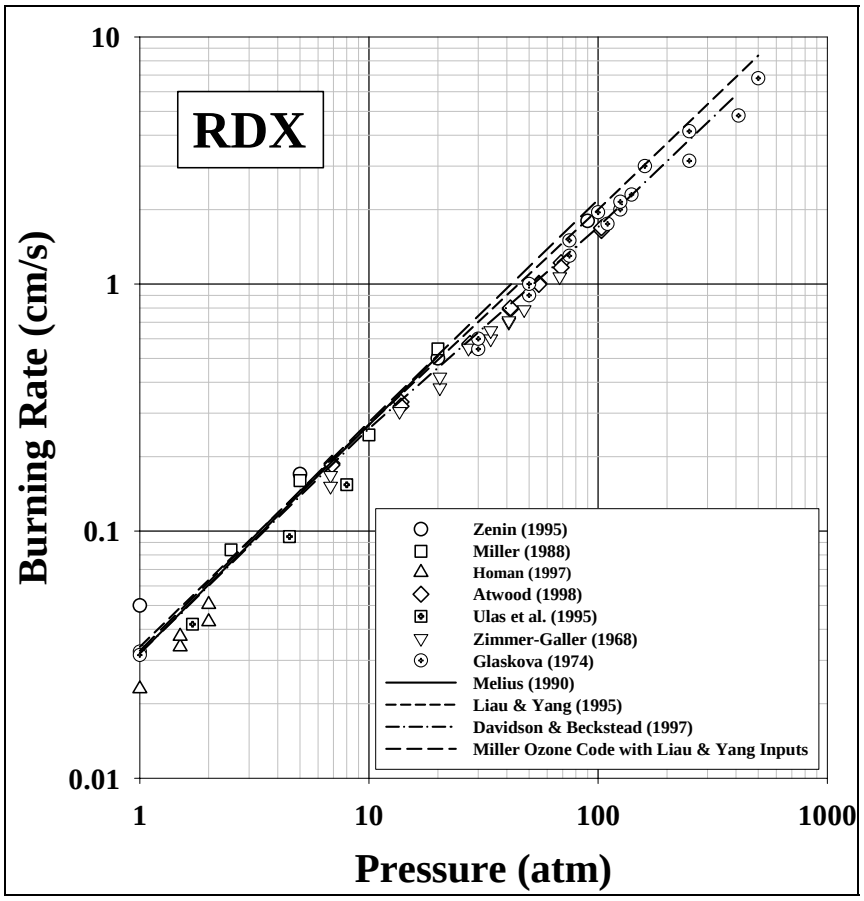

Figure 8. Several 3-phase models compared to experimental RDX burning rates.

In the final analysis, no definitive comparison is possible because of the incomplete reportage of input data used in the Melius (*18*), Liau and Yang (*4*), and Davidson and Beckstead (*5*) models. Although each of the models based their solution of the gas-phase conservation equations on the PREMIX code (*28*) developed at Sandia National Laboratories, they each implemented the 3-phase numerical solution in different ways. None of the authors described these methods in sufficient detail to enable others to reconstruct them unambiguously. One is left with the inescapable conclusion that the close agreement between models and experiment in Figure 8 is not as astonishing as it first seems but the result of finding a combination of input parameters that works. In the end, reconciliation of these various model assumptions, input data, and numerical approaches is probably not productive because of the fundamental and, so far, irreducible uncertainties associated with the condensed-phase processes, principally, but not limited to, the

Table 2. Comparisons among RDX models of selected features at 1 atm.

Model	T_s (K)	Vapor Pressure (atm) at 600 K	Sensitivity of Burning Rate to Vapor Pressure	RDX Fraction Decomposed in Liquid Phase (%)
Melius (*18*)	549	Not reported	Not reported	4.7
Liau and Yang (*4*)	573	0.69	High	<1
Davidson and Beckstead (*5*)	595	0.17	Low	25
Miller (*10*)	633	0.69	High	0

chemical reactions. Modeling the condensed phase in the kind of detail attempted by Liau and Yang and Davidson and Beckstead is not currently supported by the availability of adequate experimental measurements and may never be.

4.4 Multi-Ingredient Propellant Mixtures: A New Approach

In view of the situation previously described, how can one go beyond a relatively simple propellant ingredient like RDX, which has been the subject of the most extensive modern research to date, to treat multi-ingredient propellants? I asked this question of myself 6 years ago and in seeking an answer had an idea which became the basis for launching a new approach. The idea was to construct a hybrid-rigor model in which the gas phase would be treated in full elementary-reaction detail but the condensed phase and surface gasification would be treated in semi-empirical fashion using the Arrhenius-like expression first used by Rice and Ginell (*7*) and known in the propellant community as the "pyrolysis law":

$$\dot{m}(T_s) = A_s e^{-\frac{E_s}{RT_s}} \quad , \tag{36}$$

coupled with a set of hypothesized decomposition products from each propellant ingredient. The decomposition products would conform to proper chemical balance and be selected according to available experimental results and theoretical reasoning. Furthermore, each propellant ingredient would be assumed to decompose without interference from other ingredients (i.e., noninteractively). A full development of this model for nitrate-ester propellants is given elsewhere (*29*, *30*), but the basic concepts will be discussed here.

Of course, if one had to measure a pyrolysis law for every combination of ingredients, there would be no hope of predictive capability from such a model. However, Anatoli Zenin, having spent the last 40+ years refining the technique of measuring surface temperatures of numerous propellant mixtures and single propellant ingredients with microthermocouples, discovered that a single, universal pyrolysis law (*23*) (Figure 9) holds for a wide range of double-base propellant

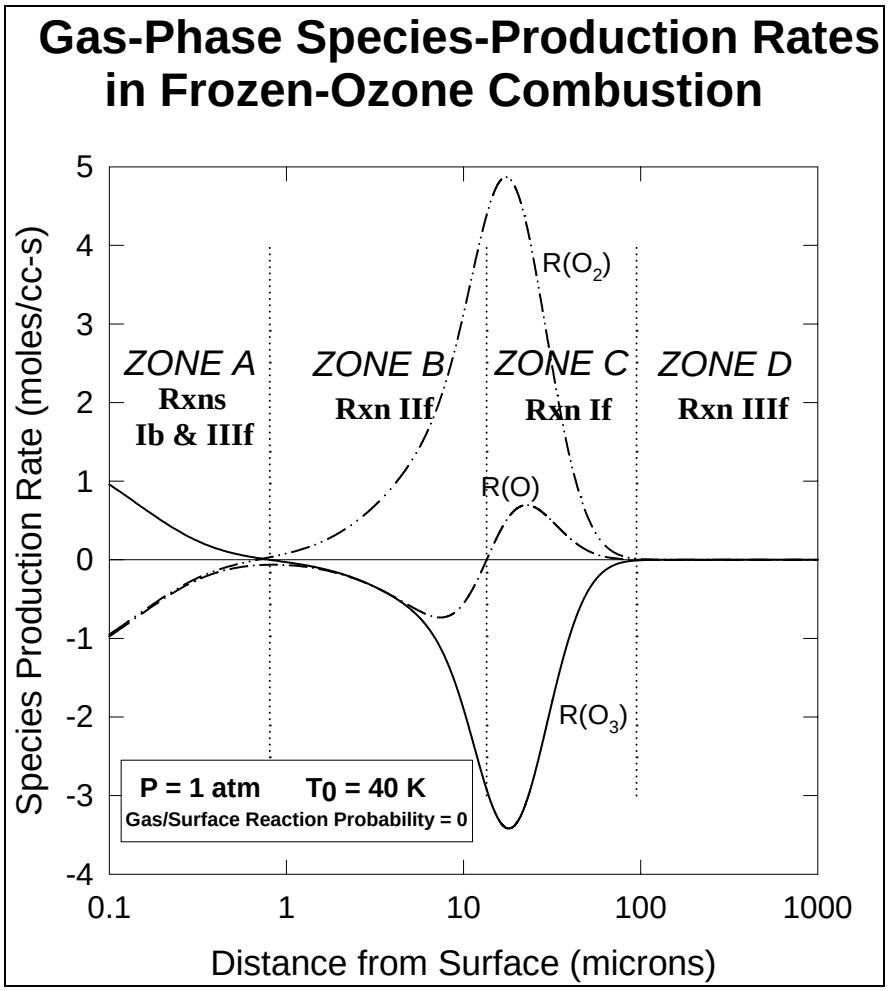

Figure 9. Zenin's universal pyrolysis law with sampling of his experimental data (*23*) for a wide range of double-base propellant ingredient proportions.

formulations with NG content from 0% to 50% and NC with percent nitration from about 11.5% to 13.5%. As seen in Figure 9, even extreme initial temperature data are reasonably well accommodated by the same pyrolysis law. Furthermore, the same double-base pyrolysis law also works for additions of HMX (*23*). I wondered if other classes of ingredients (e.g., nitramine-binder systems) might display this same universality. If so, this idea might lead to a predictive tool, at least for members of these classes. To test this hypothesis, Zenin (*23*) applied his embedded microthermocouple technique to a wide range of nitramine-oxidizer/polymeric-binder combinations (Table 3). Figure 10 shows the results of this work (*31–33*) to date. First of all, notice that there is little difference between RDX and HMX materials with the same binder. Also, most binders with RDX and HMX oxidizers group closely about the pyrolysis law labeled RDXBA, which was obtained as a least-squares fit to the RDX/poly 3,3-bis(azidomethyl) oxetane (BAMO)-poly 3-azidomethyl-3-methyl oxetane (AMMO) data alone. It is of great interest that the CL20/PUNE results, while closely adhering to the form of the pyrolysis law, occupies a very different region on the graph. HMX/PUNE, on the other hand, is in excellent accord with the

Table 3. Zenin's nitramine/binder test-material formulations (*31–33*).

Test-Mixture Designation	Binder-Ingredient Proportions	Oxidizer-Binder Proportions
RDX (or HMX)[a]/BAMO-AMMO	50:50	80:20
RDX (or HMX)[a]/BAMO-THF	50:50	80:20
RDX (or HMX)/CBIH	—	80:20
RDX (or HMX)/GAP1U	—	80:20
RDX (or HMX)/GAP2	—	80:20
CL20 (or HMX)/PUNE	20:80	70:30

[a] 50% by weight of particle sizes < 50 μs, 50% in range 150–300 μm, 99% purity of RDX and HMX.

Notes:
THF = tetrahydrofuran.
CBIH = copolymer of butadiene and isoprene with hydroxyl terminated groups.
GAP1U = glycidyl azide-polyurethane copolymer.
GAP2 = glycidyl azide polymer (molecular mass of 2000).

RDXBA pyrolysis law. The reason for this difference is not known; perhaps, the rate-limiting step in the decomposition of CL20 is significantly different than for RDX and HMX. The tentative conclusion from these measurements is that propellants composed of RDX or HMX in both inert and energetic polymeric binders do indeed follow a universal pyrolysis law. CL20 clearly follows such a law for one energetic binder and may for other binders as well. Other binders are currently being investigated. The parameters for these pyrolysis laws along with Zenin's double-base law are given in Table 4. It would be of considerable practical interest to explore the theoretical basis for the existence of these universal pyrolysis laws; they seen to suggest a common rate-limiting step associated with the condensed phase and/or interfacial region for each family. An understanding of this behavior could well lead to a predictive capability for pyrolysis laws, thereby removing a large empirical component in the present model.

By way of reinforcing the general applicability of the form of the pyrolysis law, equation 36, it is worth noting that neat RDX, HMX, and ammonium dinitramide (ADN) all may be well described by this same functional relationship, as can be seen in Figure 11. In addition to the experimental data, I have plotted in Figure 11 the results of a least-squares fitting of the pyrolysis law to results calculated using my 3-phase code for both frozen ozone and neat RDX. It can be seen that the relation between the calculated surface temperatures and burning rates are in excellent accord with the form of equation 36. In view of all the foregoing evidence, there is considerable support for the general applicability of the pyrolysis law, and this should encourage efforts to calculate the parameters from first principles, an important step in removing the empiricism from this modeling approach and opening the door to much wider prediction capability.

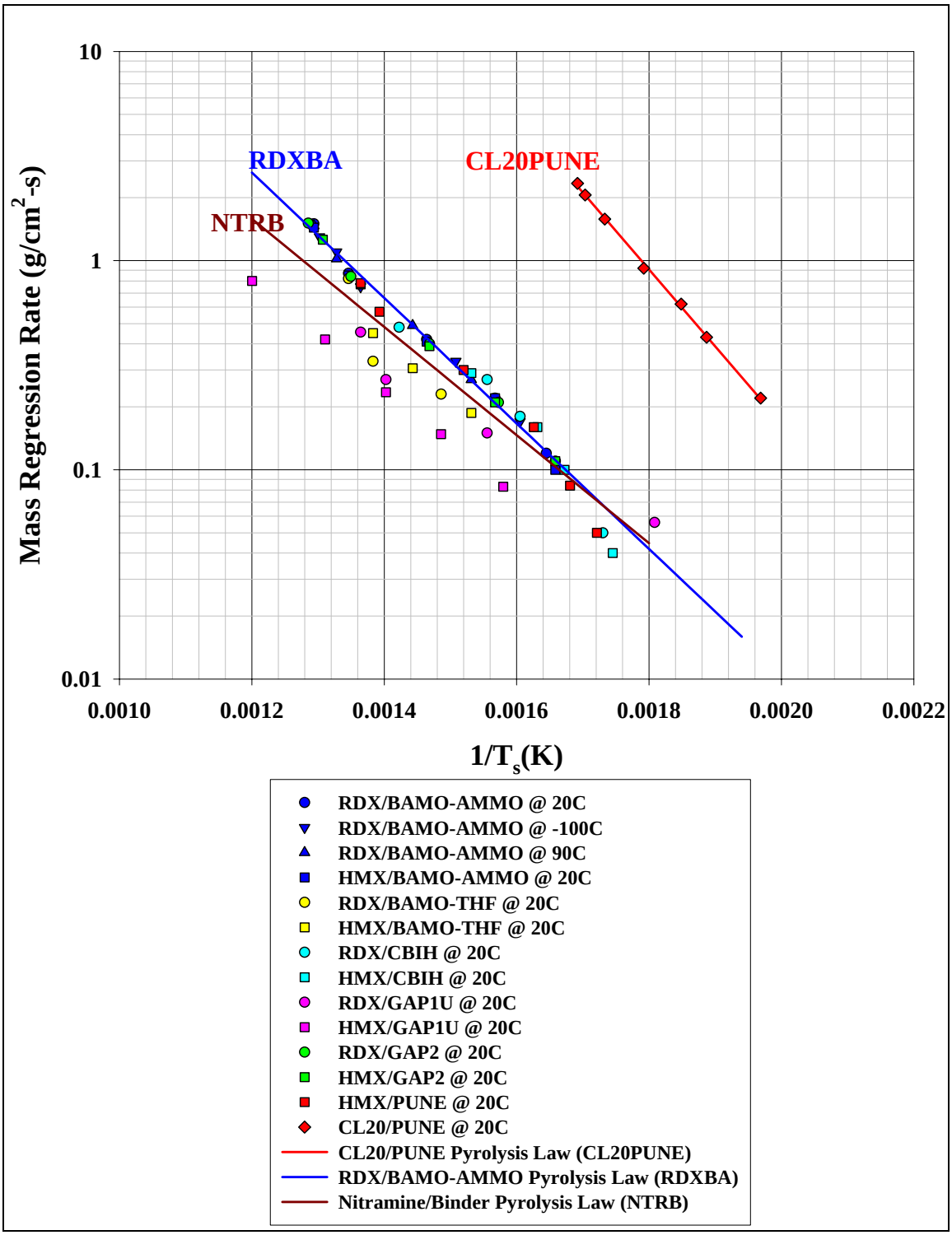

Figure 10. Zenin's data for a wide variety of nitramine/binder combinations (*31–33*). The pyrolysis law identified as NTRB is a least-squares fit to all of the RDX/ and HMX/binder data. The RDXBA pyrolysis law is a fit to the RDX/BAMO-AMMO data alone, and the CL20PUNE pyrolysis law is the least-squares-fit to the CL20/PUNE data alone.

Table 4. Parameters for various pyrolysis laws, equation 36.

Designation	A_s (g/cm^2-s)	E_s (cal/mol)
DB	1800	9935
RDXBA	10470	1371
NTRB	2004	11827
CL20PUNE	1.868×10^6	16032

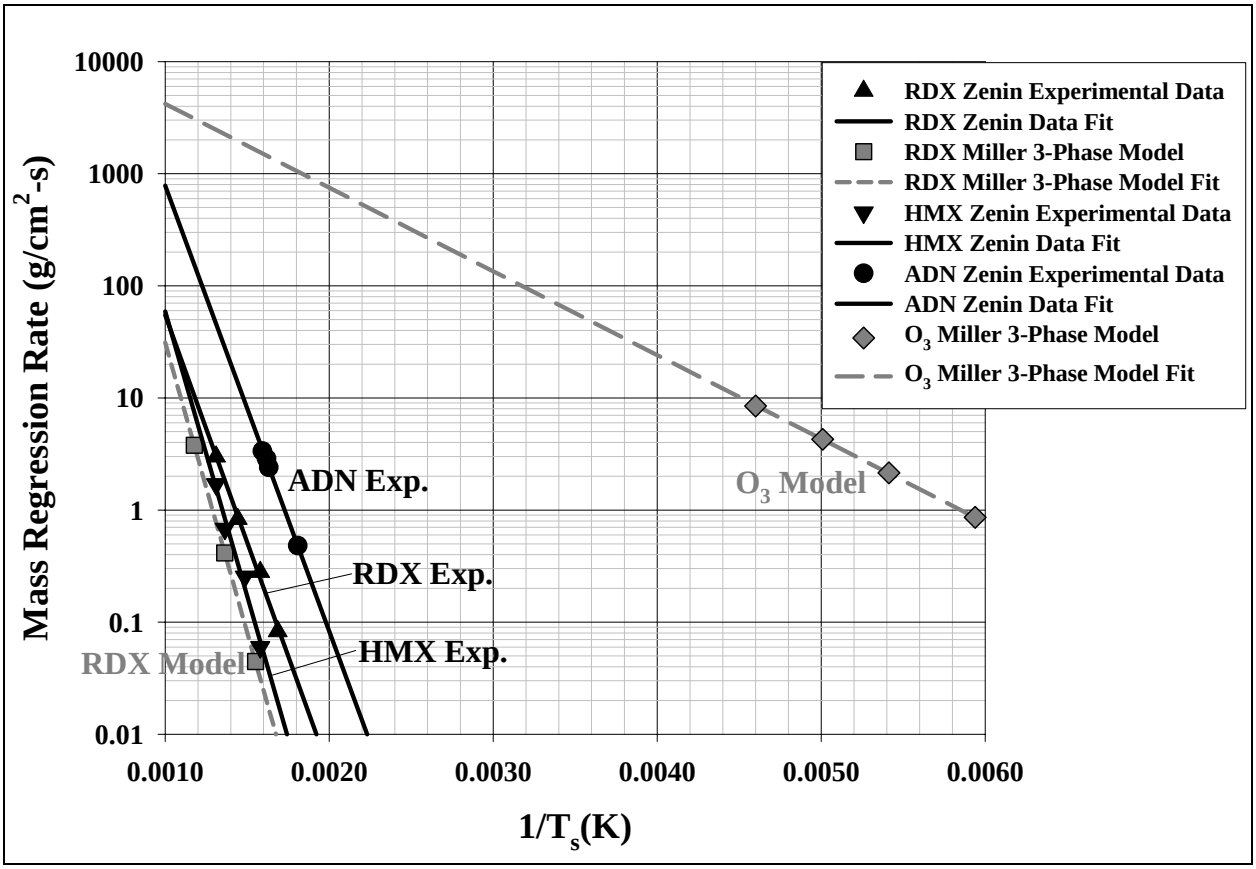

Figure 11. Pyrolysis laws for a number of neat energetic materials. The RDX Miller calculation was performed with the 3-phase model previously used for frozen ozone using the same input data for RDX as Liau and Yang (with the exception of no condensed-phase reactions). All data and calculations are for an initial temperature of 293 K except for frozen ozone, which was at 40 K.

As previously indicated, the model requires the identity and mole fractions of the chemical species resulting from the condensed-phase processes (i.e., the gases leaving the surface). These species will be far from the equilibrium distribution, and, therefore, one has only chemical balance to constrain the set of surface products absolutely. With ingredients as complex as those for propellants, this means that there are usually very many possible product sets to consider. Experimental thermal decomposition studies may be useful guides to selecting an appropriate

product set but not perfect since those experiments may not accurately mimic the conditions of the burning surface (temperature and heating rate) and probably all suffer from significant unknown changes in the surface products as a result of very fast reactions close to the surface. Use of general theoretical reasoning can also help limit the number of probable product sets. In the end, however, an important selection criterion must be whether the proposed product set results in a calculated burning rate close to the experimental one. Use of this criterion, of course, assumes that the pyrolysis law, the gas-phase reaction mechanism, and all the other input data the model needs are accurate. The predictive ability of the model for the whole propellant is redeemed by insisting that the decomposition products from each ingredient, "calibrated" ideally for that ingredient alone, remain consistent for all propellant formulations using that ingredient. This strategy is probably the best-compromise approach, but one should recognize that the assumption of non-interactivity in decomposition might be a better approximation for some systems than others.

Since all fielded gun propellants include at least some NC and certain propellants, such as M10, have 98% NC, any burning-rate model of practical importance will have to deal with NC as an ingredient. Not only is NC a complex long-chain polymer, but the repeat units vary among four different types depending on whether the glucose ring is triply, doubly, singly nitrated or unnitrated altogether. Figure 12 shows a triply nitrated repeat unit. NC is characterized for propellant use by its average percent nitrogen (%N) by weight, and this quantity varies typically from ~11.5 to ~13.5 %N. Pure cellulose trinitrate, cellulose dinitrate, and cellulose mononitrate have 14.14, 11.11, and 6.76 %N, respectively. The work of Leider and Seaton (*34*) showed that a 12.3 %N NC has all three nitration states present but no unnitrated sites. We developed a Monte Carlo model (*29, 30*) to determine for an NC specimen of given percent nitrogen what is the distribution among these three nitration states. Predictions of this model are compared to the nuclear magnetic resonance (NMR) data of Todd and Glasser (*35*) in Figure 13. The burning-rate model then assumes that NC consists of three separate, hypothetically pure ingredients corresponding to cellulose tri-, di-, and mononitrate in the proportion indicated by the Monte Carlo model. The densities of these hypothetically pure nitrates are obtained from a MD calculation (*36*) using the COMPASS force field.

The model handling of multi-ingredient propellants is summarized graphically for JA2 in Figure 14. This figure does not represent the current decomposition-product sets but serves to illustrate the principles behind the method. The CYCLOPS (*29*, *30*) code, named for the mythical race of creatures who forged thunderbolts for Zeus, is the computer-code embodiment of the burning-rate model under discussion. CYCLOPS accepts the weight percents of each ingredient and checks to see if NC is among them. If so, then the Monte-Carlo subroutine is called and the nitrate state distribution determined. The ingredient list is then expanded to include the three NC subingredients (cellulose tri-, di-, and mononitrate). The condensed-phase decomposition

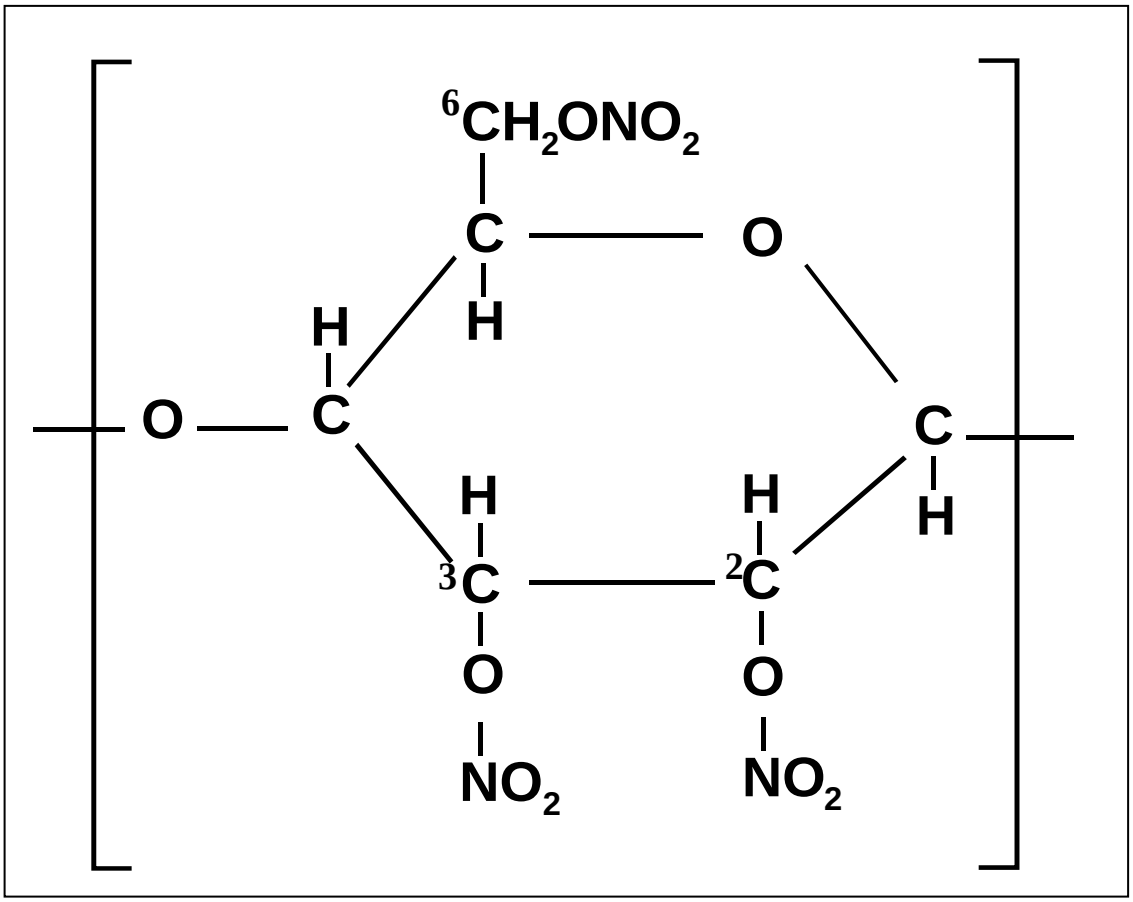

Figure 12. Triply nitrated NC repeat unit.

products for each of the ingredients on the expanded list are then obtained from the decomposition-products database, and the net set of products computed according to the proportion of each ingredient. A trial value for the linear burning rate is then read in from the problem input file and converted to mass flux using the code-computed propellant density. The surface temperature for this mass flux is then computed from the pyrolysis law, and these values are passed to a modified version of the PREMIX (*28*) code, which is called as a subroutine to solve the gas-phase conservation equations. From this solution the heat feedback to the surface is computed and compared with the heat feedback required to transform the propellant ingredients at their initial temperature to the condensed-phase decomposition products at the trial surface temperature using the trial mass flux. New trial values are automatically provided by the code until the two heat fluxes are in satisfactory agreement. The criterion for convergence is actually expressed in terms of acceptable changes in successive guesses of the mass flux, which is the unknown sought.

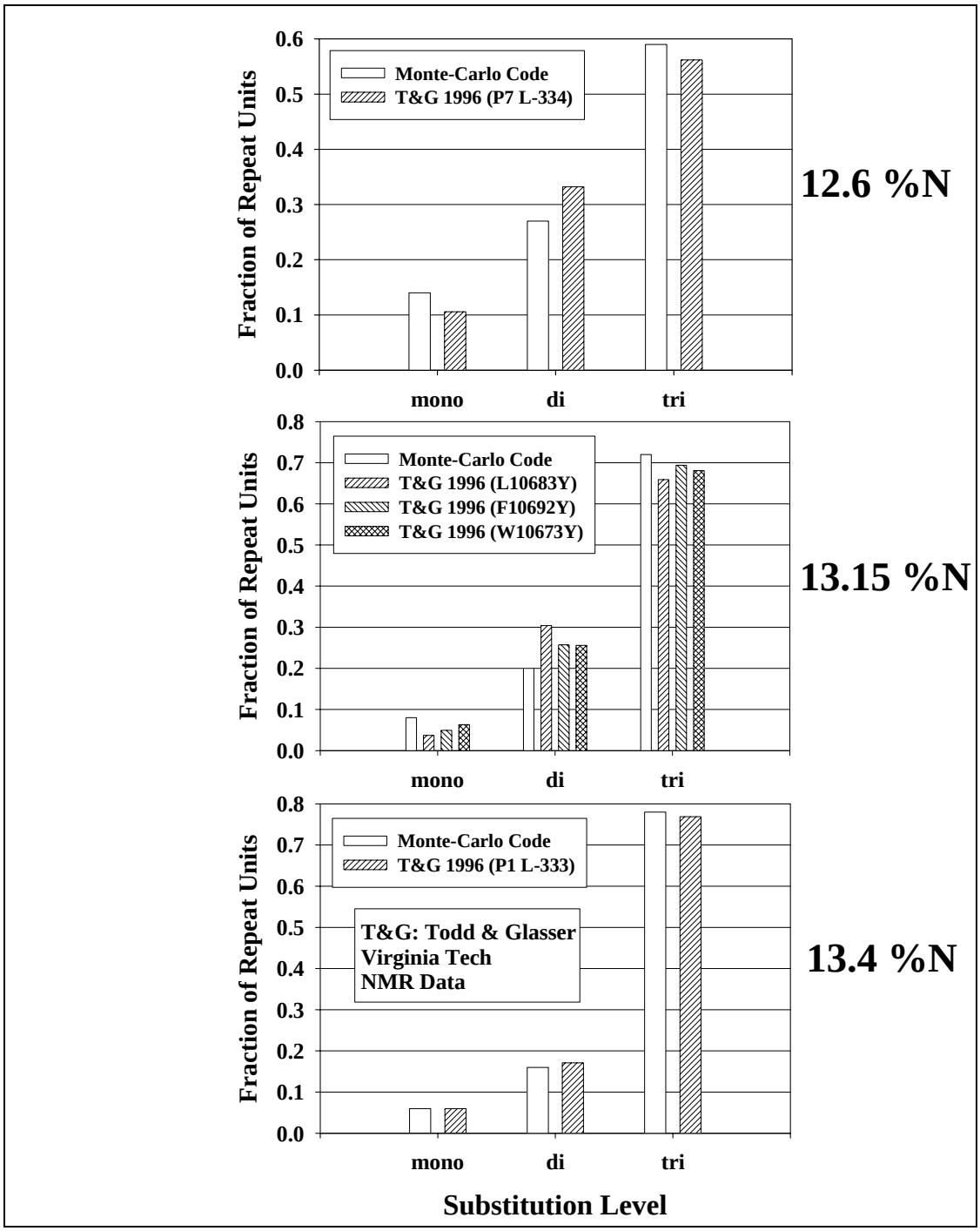

Figure 13. Monte Carlo model for distribution of repeat units among cellulose tri-, di-, and mononitrates for an NC specimen of given percent nitrogen. Comparison is made of the model predictions with the NMR data of Todd and Glasser (*35*).

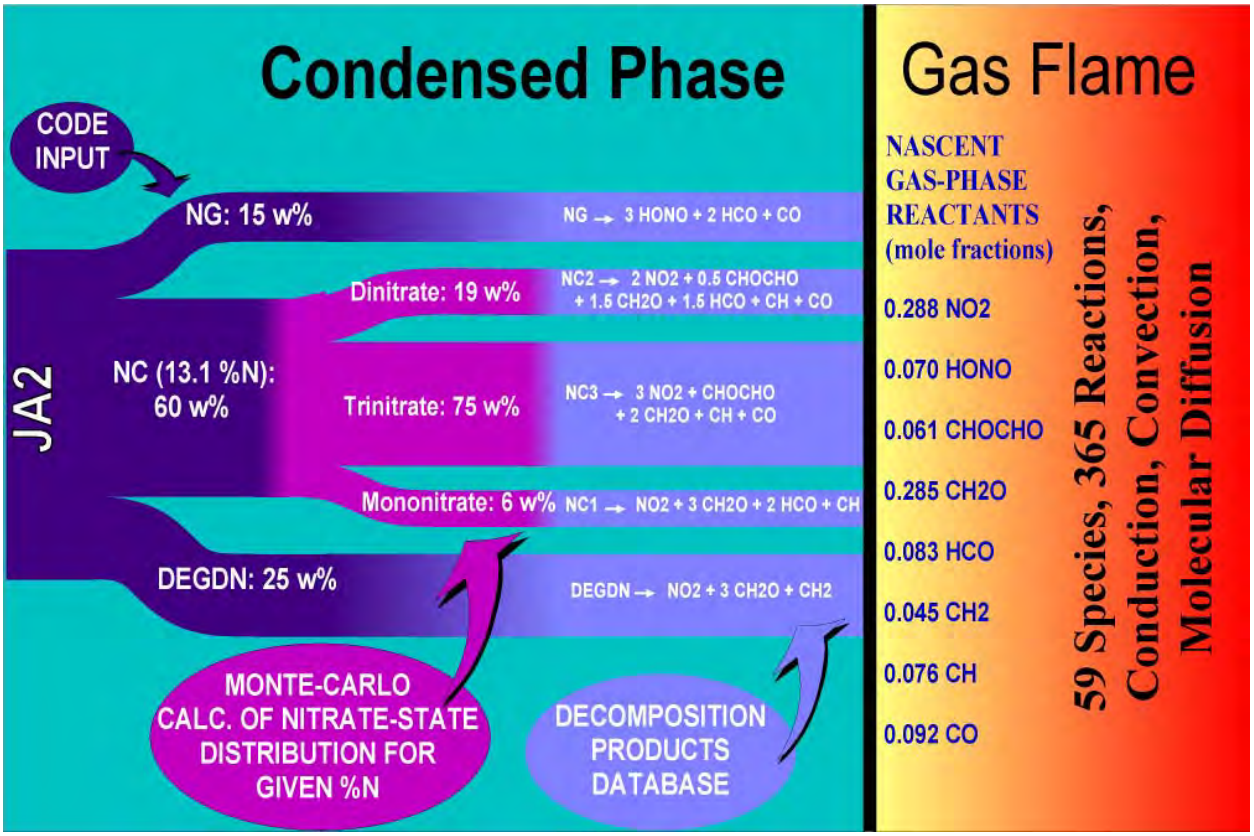

Figure 14. Conceptual deconstruction of a propellant containing NC into subingredients and then into net condensed-phase decomposition products entering the gas phase.

Results for the burning rate of M10 and JA2 are shown in Figures 15 and 16 compared to the experimental data of Miller (*22*), Juhasz (*37*), and Atwood et al. (*38*) for M10 and Miller (*22*) and Juhasz et al. (*39*) for JA2. An extensive analysis (*29*, *30*) of the chemical-kinetic origin of the inflection in the M10 curve has been made. It was discovered that those reactions controlling the dark-zone length at low pressures (<10 MPa) have little influence over the burning rate at low pressures, but, to our surprise, a major effect on the burning rate at high pressures, where a dark zone does not even exist. Thus, studies of the dark-zone chemistry experimentally accessible at low pressures actually are probing those reactions with critical influence over the burning rate at high pressures. This finding provides new impetus to experimental dark-zone investigations, especially for nitramine propellants because their dark-zone chemistry is less well known than that of nitrate-ester propellants. How well CYCLOPS predicts the structure of the dark zone is shown in Figure 17, where the temperature and NO profiles are seen to compare very favorably with experiment. Table 5 gives a comparison of predicted and measured major species for a double-base propellant similar to M9; again, the agreement is excellent. The experimental measurements used for comparison are those of Heller and Gordon (*40*), Lengelle et al. (*41*), and Vanderhoff et al. (*42*), and they were renormalized for direct comparability by Vanderhoff et al. (*42*).

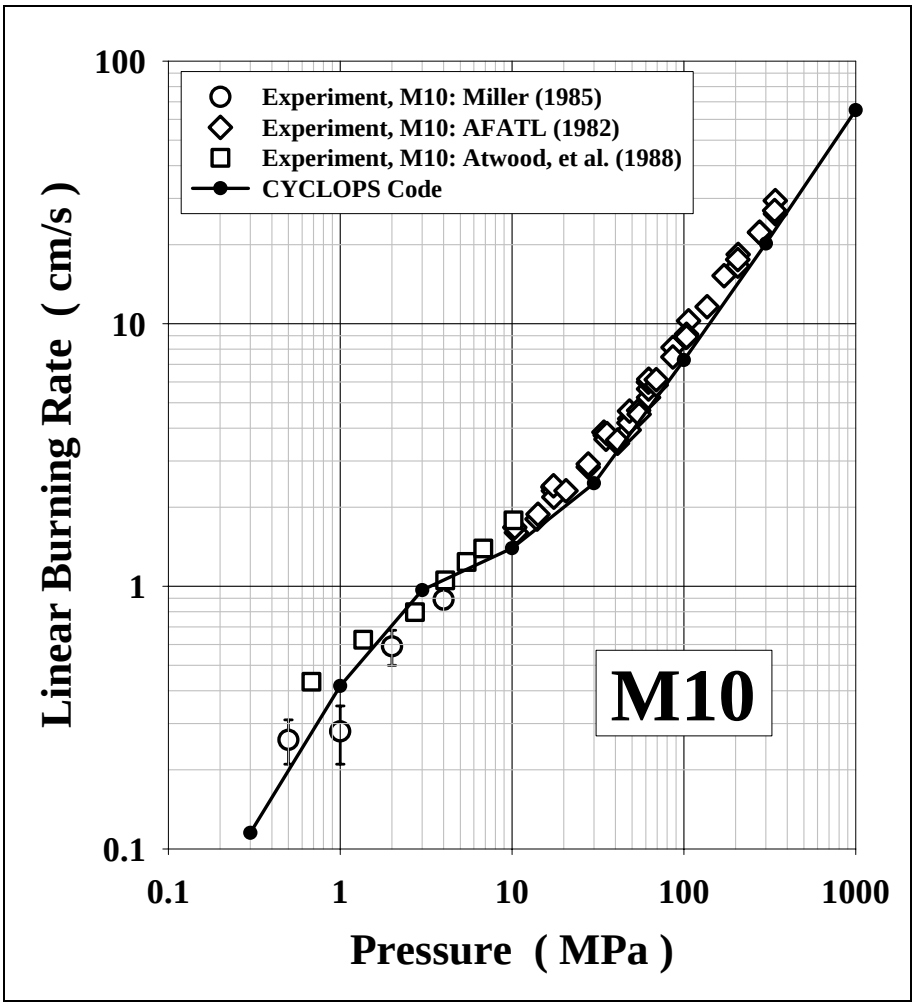

Figure 15. Comparison of CYCLOPS-code calculations of burning rate of M10 propellant with experimental data.

A final example is given of more recent work (*43*) on RDX in an energetic thermoplastic elastomer (ETPE) binder. The excellent comparison with experimental burning-rate data shown in Figure 18 is tempered by the poor prediction of the thermal structure in Figure 19. This inconsistency might at first be thought to suggest that the good burning-rate prediction is simply fortuitous, but this is not necessarily the case. As we learned in the case of M10, the burning rate and the dark-zone length at low pressure may be controlled by different sets of reactions, so it is possible that the good burning-rate prediction and poor thermal structure prediction may be due to imperfections in the chemical mechanism describing the nitramine dark-zone chemistry. In all propellants with RDX, we assume that the RDX evaporates unchanged, just as I had assumed for neat RDX; however, binder ingredients are assumed to decompose in the condensed phase.

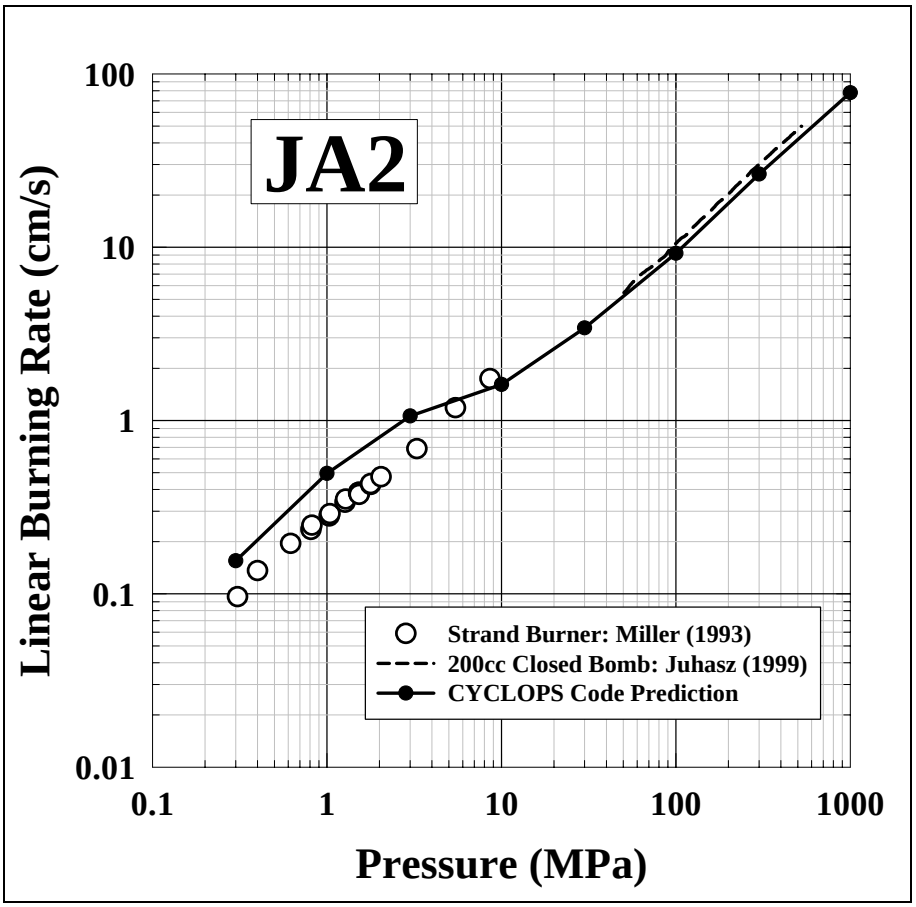

Figure 16. Comparison of CYCLOPS-code calculations of burning rate of JA2 propellant with experimental data.

The foregoing examples give evidence of the promise of the CYCLOPS code in providing both reasonable predictions of burning rate as well as details of the gas-phase flame structure and detailed chemistry. At present, the code is limited to certain families of propellant ingredients, but the number of families will likely increase as other systems are studied. However, perhaps more important is the growing probability that one might be able to predict pyrolysis laws from first principles considerations. Certainly, greater theoretical capabilities to predict the final condensed-phase decomposition products of propellant ingredients can be brought to bear. Thus, the CYCLOPS code may well provide the best computational vehicle for incorporating results of new theoretical approaches to the condensed-phase and surface processes. How this might be accomplished while maintaining mathematical tractability of the code is suggested in section 5.

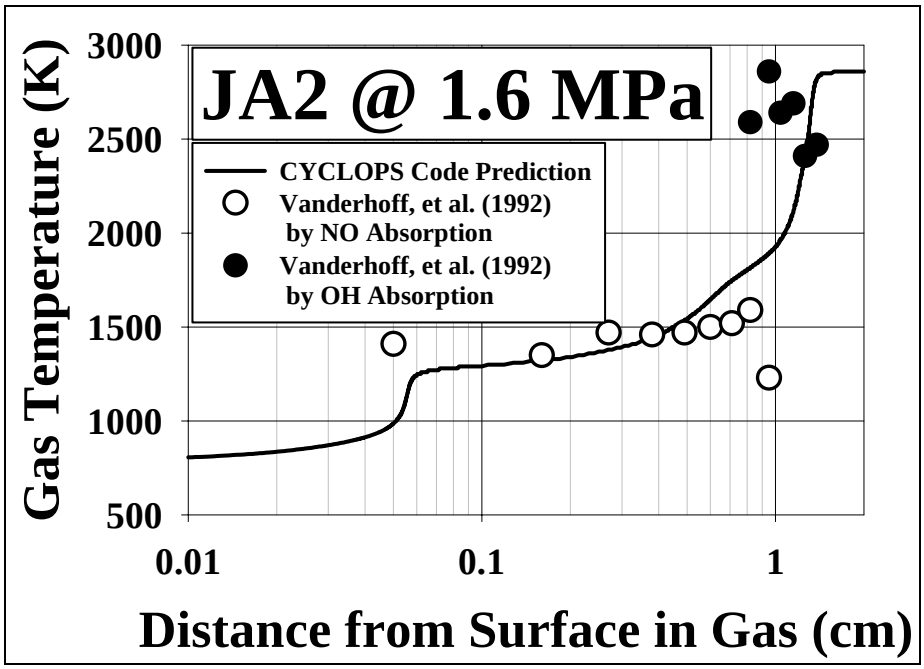

Figure 17. Comparison of CYCLOPS-code predictions of dark-zone thermal structure compared with the experimental data of Vanderhoff et al. (*42*)

Table 5. Comparison of major species mole fractions in the dark zone of double-base propellant with various experimental measurements.

Parameters	Heller and Gordon[a]	Lengelle et al.[b]	Vanderhoff et al.[c]	CYCLOPS (Present Model)
P (MPa)	1.6	0.9	1.7	1.7
Dark-zone temperature (K)	1600	1500	1500	1543
NO	0.24	0.21	0.24	0.25
CO	0.33	0.38	—	0.32
H_2	0.08	0.08	—	0.08
N_2	0.04	0.02	—	0.004
H_2O	0.20	0.20	—	0.19
CO_2	0.10	0.09	—	0.10
HCN	0.004	—	—	0.004
CH_4	0.008	0.026	—	0.009
C_2H_4	0.008	0.008	—	0.001

[a] Source: (*40*).
[b] Source: (*41*).
[c] Source: (*42*).

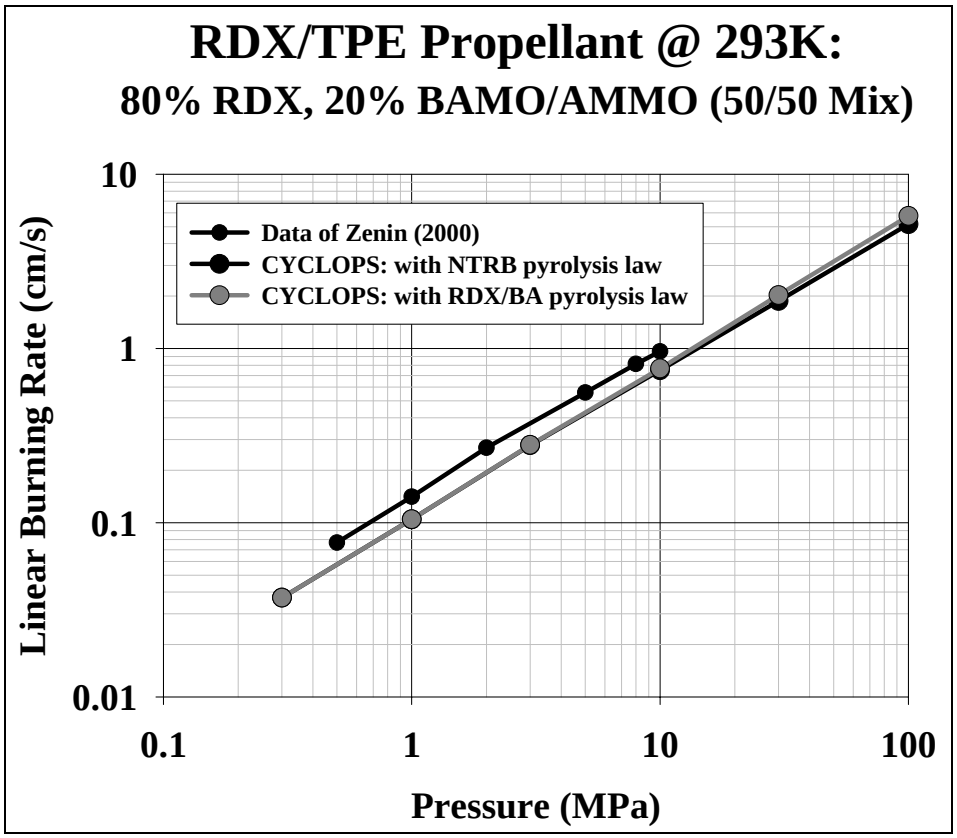

Figure 18. Comparison of CYCLOPS-code calculations of the burning rate of and RDX/thermoplastic elastomer (TPE) propellant using two different pyrolysis laws with the experimental data of Zenin (*32*).

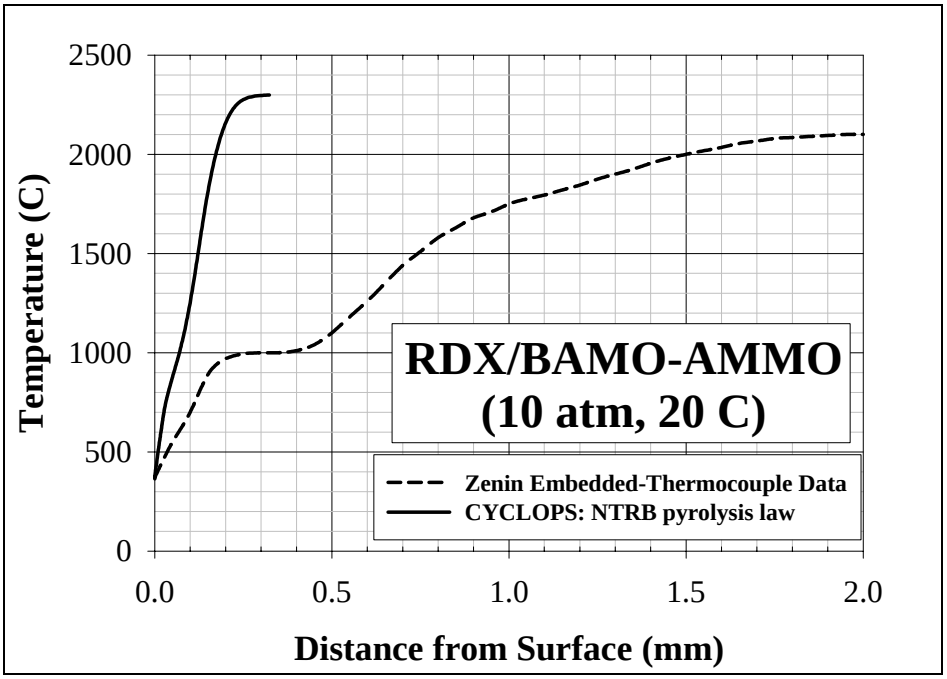

Figure 19. Comparison of CYCLOPS-code predictions of dark-zone thermal structure for an RDX/TPE propellant with the microthermocouple data of Zenin (*32*).

In summary, the CYCLOPS code is based upon a few simple propositions:

- The surface regression may be adequately idealized as 1-D. This condition is probably met for most homogeneous propellants. It may also be approximately true for many composite propellants where the burning rate is not a strong function of oxidizer particle size. Surface melt layers, for example, may provide effective premixing of ingredients where the oxidizer particle sizes are not too large.
- The surface regression may be described by a pyrolysis law, equation 36. I have shown that this condition has been met by a large number of neat energetic materials and mixtures of typical propellant ingredients.
- The overall products of condensed-phase decomposition may be estimated with sufficient accuracy. Chemical balance and results of thermal decomposition experiments are sources of guidance here, though only the former can be considered as an absolute constraint because of the high probability of secondary reactions in decomposition experiments.
- The decomposition of one propellant ingredient does not affect the decomposition of other ingredients, i.e., the decomposition of a multi-ingredient propellant may be described as the superposition of the independent decompositions of each of its ingredients. This may well be a better approximation for some ingredients than for others. Short of describing the mixture decomposition theoretically on a molecular scale, there is little recourse to this assumption. However, it is often found that significant changes in detailed combustion mechanisms have a remarkably weak influence on the burning rate, that quantity being a highly integrated consequence of myriad underlying details. CYCLOPS exploits this relative insensitivity to mechanistic details.

Finally, since the CYCLOPS code is the first code of its kind (though still undergoing development to improve robustness for general use), one can anticipate ways in which it might be put to practical use even at its current stage of development. First, the CYCLOPS code can be used to optimize ingredient proportions to achieve a target burning rate. Also, CYCLOPS could be used to explore subtle, previously unexplained effects of formulation on burning rate. For example, German-made JA2 burns about 20% faster than U.S.-made JA2 with identical ingredient *proportions*. However, the two differ by different specifications on the NC component. While the average percent nitrogen for the two propellants is the same, the two materials are made from blends of two lots of NC with different percent nitrogen. Because our nitrate-state-distribution Monte Carlo code predicts that the surface products for these two propellants will be different, it will be worthwhile to see if CYCLOPS can predict the burning-rate difference. Further, CYCLOPS could be used to help set manufacturing tolerances in the specifications of ingredient proportions in military propellants. The CYCLOPS code could be used to determine how any given set of tolerances will map into variations of the burning rate and these burning-rate variations could be judged by using them as inputs to interior-ballistic codes. The burning rate at low pressure has been shown to be sensitive to the heats of formation of propellant ingredients in

certain cases (*29*, *30*). To the extent that ingredient purity is reflected in the heat of formation (e.g., due to dinitroglycerine impurity in trinitroglycerine), the CYCLOPS code could be used to determine how ingredient purity affects the burning rate, thereby enabling rationalization of quantitative tolerances for these ingredients. Finally, the CYCLOPS code could determine the effect of chemical modifiers on the burning rate without mixing chemicals. Though not replacing the need to mix and test, using the code as a screening agent and test bed for ideas could improve efficiency and possibly suggest new compounds to test.

5. Challenges and Opportunities

The semi-empirical aspects of the CYCLOPS code need be tolerated only until theoretical advances obviate their necessity. The next level of improvement may well come from MD descriptions of the condensed phase and surface phenomena. However, this more fundamental level of treatment will have its own set of approximations and limitations. In order to deal with condensed-phase reactions, for example, considerable progress will have to be made in the parameterization of, and experience with, reactive force fields. In my judgment, one will never want to treat the gas phase, with its dozens of species and hundreds of reactions, in this way. To do so would discard more than 50 years of hard-won kinetics research gains. One will therefore be faced with merging the discrete and continuous descriptions into a single, tractable mathematical entity. I believe that this will be no easy task, as the MD approach is inherently time-dependent with (computationally intensive) explicit statistical averaging and the steady-state continuum-mechanics approach outlined earlier in this work is inherently time-independent with implicit statistical averaging. The most fruitful approach may be to develop simple, idealized continuum submodels calibrated to stand-alone MD models of a limited set of phenomena. For example, a reactive-MD model of the condensed phase would provide a set of condensed-phase decomposition products needed by the CYCLOPS code. Similarly, an MD model of multicomponent evaporation and/or pyrolysis could be used to determine a pyrolysis law for CYCLOPS. Results of the continuum submodels, depending on their scope, could then be easily incorporated into either a 3-phase model or a code such as CYCLOPS, retaining mathematical tractability and efficiency. Since, prior to the development of CYCLOPS, I had made a start on incorporating multicomponent evaporation into our 3-phase code, it will be used as an example here of the proposed approach.

5.1 "Molecular" Continuum Model of Multicomponent Evaporation

I consider that a molecule evaporating from a liquid surface (Figure 20) is at some distance d above the surface. I further assume that the molecule follows a tubular path from deep within the liquid to points outside the liquid; the tube has radius a_0. The conception here is that the radius of the tube is of the order of the "radius" of the escaping molecule, and what is a tortured path geometry in reality is idealized as straightened to a cylindrical path. Since the escaping molecule

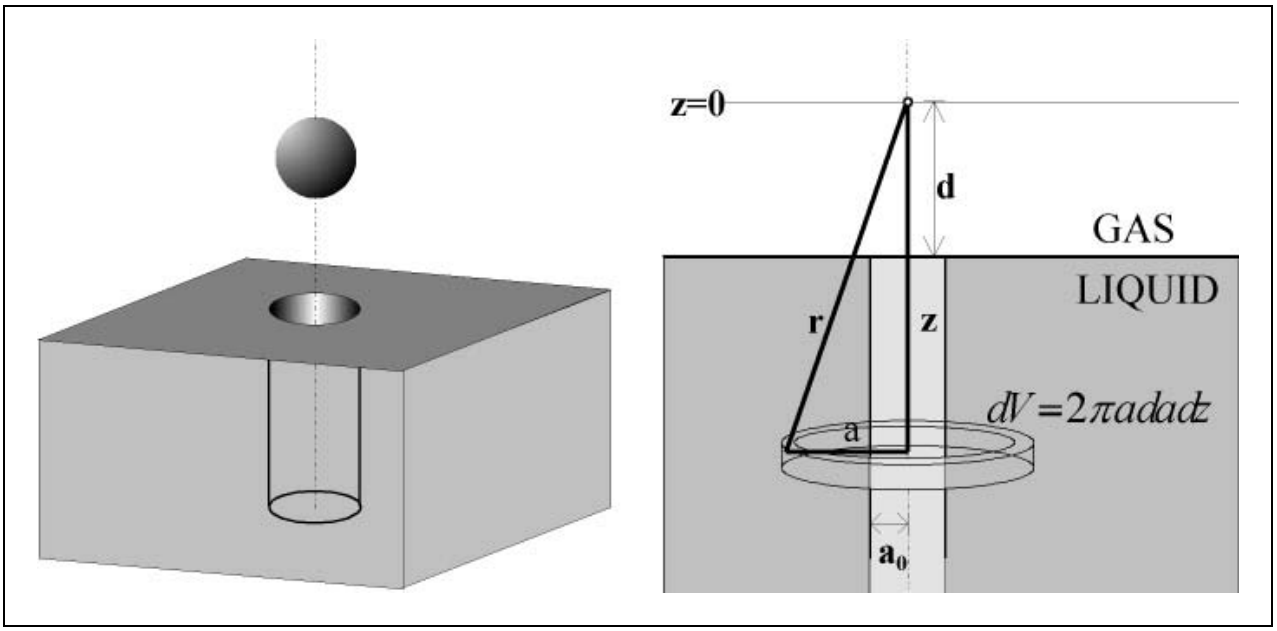

Figure 20. Model for continuous-phase molecular forces experienced by a molecule evaporating from a liquid surface.

is at a distance *r* from all the molecules in the differential volume element, $dV = 2\pi\, a\, da\, dz$, the potential energy of interaction is $d\Phi = \phi(r)\, n\, dV$, where *n* is the number density of liquid molecules (Figure 20). If I assume a Lennard-Jones (L-J) interaction potential, where ε is the well depth and σ is the collision diameter, i.e.,

$$\phi(r) = 4\varepsilon\left[\left(\frac{\sigma}{r}\right)^{12} - \left(\frac{\sigma}{r}\right)^{6}\right], \tag{37}$$

and integrate over all the molecules in the liquid, one obtains

$$\Phi(d) = 8\pi n_{Liq}\varepsilon\sigma^2\left\{\frac{1}{10}\left(\frac{\sigma}{a_0}\right)^9 f[x(d)] - \frac{1}{4}\left(\frac{\sigma}{a_0}\right)^3 g[x(d)]\right\}, \tag{38}$$

where

$$x(d) = -\frac{d}{a_0}, \tag{39}$$

$$f(x) = \frac{x}{9}\left[\frac{9}{8(1+x^2)^4} + \frac{63}{48(1+x^2)^3} + \frac{315}{192(1+x^2)^2}\frac{945}{384(1+x^2)}\right] + \frac{105}{384}\arctan(x) + \frac{105\pi}{768}, \tag{40}$$

and

$$g(x) = \frac{x}{2(1+x^2)} + \frac{1}{2}\arctan(x) + \frac{\pi}{4}. \tag{41}$$

Two important extensions can be made to this formulation. The first is to add the effects of interaction between the escaping molecule and the gas-phase molecules. This modifies the potential to

$$\Phi(d) = 8\pi\left(n_{Liq} - n_{Gas}\right)\varepsilon\sigma^2\left\{\frac{1}{10}\left(\frac{\sigma}{a_0}\right)^9 f\left[x(d)\right] - \frac{1}{4}\left(\frac{\sigma}{a_0}\right)^3 g\left[x(d)\right]\right\}. \tag{42}$$

The other important extension is to the multicomponent case. This requires a sum over the interactions between the escaping molecule of species *i* with the other species *j*, of total different kinds, *N*. Thus, the multicomponent version of the interaction potential between an evaporating molecule of species *i* at a distance *d* from the surface and all other species both in the liquid and in the gas phase is

$$\Phi_i(d) = 8\pi\left(n_{Liq} - n_{Gas}\right)\sum_{j=1}^{N}\varepsilon_{ij}\sigma_{ij}^2\left\{\frac{1}{10}\left(\frac{\sigma_{ij}}{a_0}\right)^9 f\left[x(d)\right] - \frac{1}{4}\left(\frac{\sigma_{ij}}{a_0}\right)^3 g\left[x(d)\right]\right\}, \tag{43}$$

with its ancillary definitions in equations 39–41. These equations may seem awkward but are easily and quickly evaluated in a computer code and represent, in a very general way, enormously complex phenomena. For example, they describe quantitatively how the heat of vaporization goes to zero at the critical point, where the liquid- and gas-phase densities become indistinguishable.

A necessary test of the model is the accuracy with which the previous equations predict the heats of vaporization of pure substances. The heat of vaporization is obtained by taking the limit in the previous equations as *d* 64 in equation 38. The result is

$$H_{vap} = \pi^2 n_{Liq}\varepsilon\sigma^3\left(\frac{\sigma}{a_0}\right)^3\left[1 - \frac{7}{32}\left(\frac{\sigma}{a_0}\right)^6\right]. \tag{44}$$

Application of this model is made to 61 data sets for polar and nonpolar molecules using the compilation of L-J parameters in Reid and Sherwood (*44*) and Reid et al. (*45*). Calculation results shown in Figure 21 are obtained by performing a non-linear least-squares fit of the heat-of-evaporation experimental data to equation 44 using P_e, defined as follows, as an adjustable parameter to mediate between the raw theoretical result H_{calc} and the best estimate value H_{est};

$$H_{est} = P_e H_{calc}. \tag{45}$$

Assuming that $\left(\frac{a_0}{\sigma}\right)$ is unity, the best-fit value of P_e turns out to be 1.10. Its proximity to unity suggests that the physical basis of model assumptions are reasonable. The standard deviation of the error using the optimized value of P_e is about ±12%. This error is surprisingly small considering that the L-J potential is not generally as faithful as an exponential-6 potential for nonpolar molecules and is has even worse fidelity for polar molecules, which are abundantly

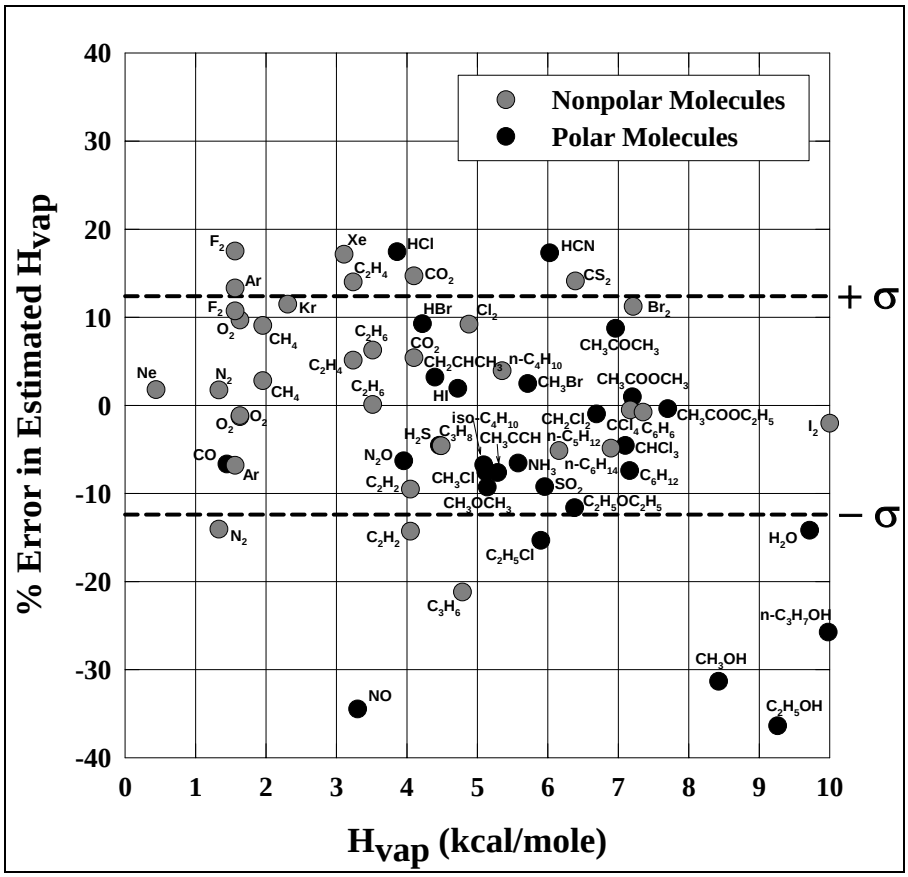

Figure 21. Accuracy of the simple heat-of-vaporization theory using 61 L-J parameter sets for both polar and nonpolar molecules.

represented in the data set. In fact, even without the adjustment parameter P_e, the standard deviation of the prediction of H_{vap} is about 16%. This good performance might be improved upon by either using another, better interaction potential or by possibly modifying the model to recognize the discrete nature of close-neighbor molecular interactions.

By itself, the previously mentioned model is not sufficient to treat the multicomponent evaporation problem. One needs also to describe the dynamics of the evaporative escape mechanism. Drawing upon kinetic theory to construct the flux of molecules leaving the liquid surface, Γ_{out}, one obtains

$$\Gamma_{out} = \frac{1}{4}\left(n_{Liq} e^{-\frac{H_{vap}}{RT_s}} \right) \bar{v}_e , \tag{46}$$

where the quantity in parenthesis is the density of molecules with energies greater than H_{vap}, and $\bar{v}_e$ is the average velocity of those molecules with enough energy to escape the heat-of-vaporization barrier. Assuming that the molecules in the surface are equilibrated at the surface temperature, T_s, it may be shown that the average escape velocity is

$$\bar{v}_e = \frac{\left(1+\beta^2 v_e^2\right)e^{-\beta^2 v_e^2}}{\beta\left[\beta v_e e^{-\beta^2 v_e^2} + \frac{\sqrt{\pi}}{2} erfc\left(\beta v_e\right)\right]}, \tag{47}$$

where

$$\beta = \sqrt{\frac{W}{2RT_s}}, \tag{48}$$

where W is the molecular weight of the escaping molecules and the minimum velocity for escape v_e is

$$v_e = \sqrt{\frac{2H_{vap}}{W}}. \tag{49}$$

The equilibrium vapor pressure is determined by equating the outward and inward fluxes at equilibrium (see arguments of section 3.3.1), i.e.,

$$p^e = \frac{4RT_s\Gamma_{out}}{\sqrt{\frac{8RT_s}{\pi W}}}. \tag{50}$$

To test the predictions of this part of the model apart from imperfections in the predicted value of the heat of vaporization, I use the experimental value of H_{vap} in the vapor-pressure formulas. With no adjustment parameters at all, the standard deviation of the predicted from experimental values is 95%. Evidently, there are more serious shortcomings in the vapor-pressure model. I experimented with several empirical modifications of the model and got interesting results by using an adjustable parameter to scale the value of H_{vap} in computing the escape velocity of equation 49. This strategy results in a standard deviation of about 36%, a much improved accuracy but possibly not sufficient for use in the multicomponent evaporation code. The best-fit scaling factor has a value of 0.68, i.e., the calculation is significantly improved by assuming that only 68% of the full heat of vaporization must be overcome in order to escape the liquid surface. These results are illustrated in Figure 22. Noting the slight downward tendency of the error with increasing H_{vap} in the figure, I tried using a two-parameter fit to the fraction of H_{vap} used to compute v_e. This improved the standard deviation slightly to 30%. The model may well be further improved and placed on a more sound theoretical basis by doing MD studies to help inform the assumptions. For example, perhaps decreasing the minimum escape velocity improves the idealized model because molecules tend to equilibrate, on average, at a value of potential energy somewhat above that in the bulk by means of collisions in the interfacial region closest to the bulk liquid. A great advantage of this bootstrapping partnership between discrete and continuum descriptions is that, by using the same model potential in both, the physics of the evaporation

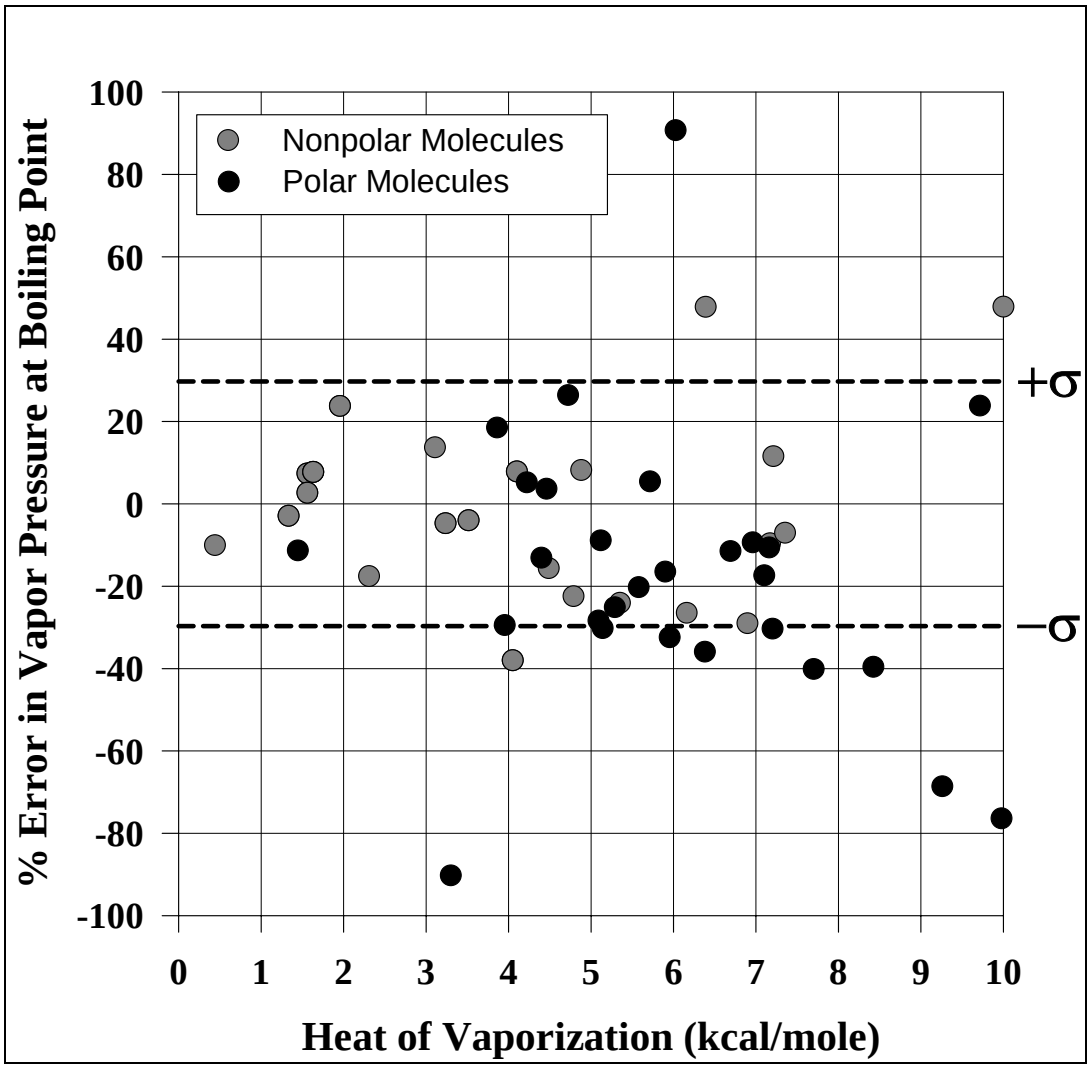

Figure 22. Accuracy of the simple vapor-pressure model using 61 L-J parameter sets for both polar and nonpolar molecules.

process can be studied and built into the continuum model apart from the behavior of any real substance. Separate studies can then address the issue of the best potential model to use. It goes without saying that the continuum models described previously can be implemented with any potential-energy function while still preserving the relatively rapid computational qualities essential to incorporation into a multicomponent burning-rate model.

One might argue that empirically based engineering correlations could do considerably better at predicting vapor pressures. In fact, I applied the Reid method (*44*, *45*) based on the corresponding-states principle to the same database of molecules used previously and found that the standard deviation was only 4%. However, these methods are apparently much less successful when applied to molecule mixtures. This may be an important limitation for energetic-material combustion, where the surface is multicomponent even for the simplest case of ozone as explained in section 3.3.2.

5.2 MD Simulations of the Condensed Phase

Another fruitful area where the MD approach has played a role and enjoys bright future prospects is in the condensed phase. An example of past use is in determining the idealized mass densities (*36*) of putatively pure polymers of cellulose mono-, di-, and trinitrate. These values are needed in the semi-empirical burning-rate model previously discussed for nitrate-ester propellants. In addition, the method was also applied (*36*) to the unreacting solid form of JA2 propellant to check the accuracy of the JA2 mass density computation by additive molar volumes, the method employed by the CYCLOPS (*29, 30*) code. Figure 23 shows a particular relaxed configuration of JA2, believed to be the first published "anatomically correct" molecular view of a real propellant. The CYCLOPS-computed value of the density is 1.56 g/cm^3, which compares very well with the MD-computed value of 1.59 ± 0.02 g/cm^3, which, in turn, compares very well with experimental value of 1.57 ± 0.01 g/cm^3.

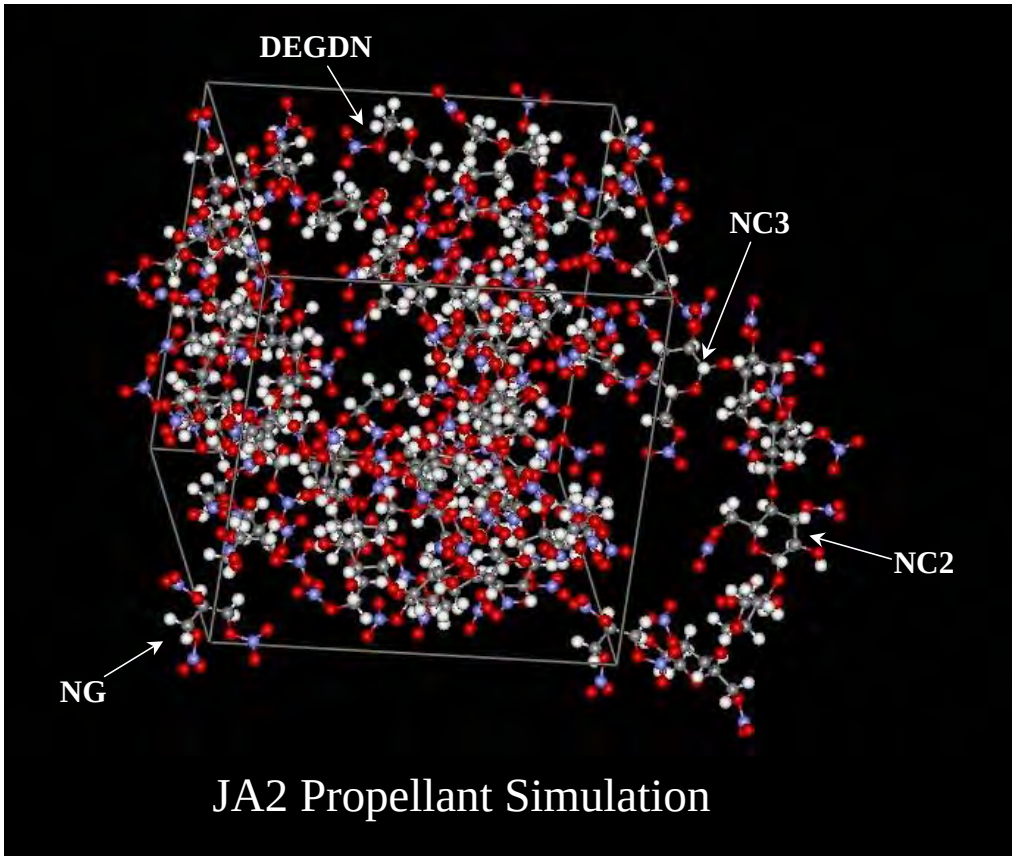

Figure 23. One view of a relaxed configuration of JA2 propellant computed by a MD simulation (*36*) consisting of 2 chains of 15 monomers representing NC, 16 molecules of diethylene glycol dinitrate (DEGDN), and 10 molecules of NG. Oxygen atoms are in red, nitrogen in blue, carbon in grey, and hydrogen in white. A number of the component molecules can be identified as indicated. This is believed to be the first computed molecular representation of a real propellant formulation.

Besides the purpose just described, such a MD simulation could be used to determine propellant heats of formation that properly account for molecular interactions between dissimilar ingredients. Currently, all such interactions are ignored for lack of computational capability and the expectation that heats of solution will generally be small, but we previously found (*29, 30*) that small changes in the heats of formation of propellant ingredients can have surprisingly large effects on the burning rate at low and intermediate pressures. This effect disappears at maximum gun pressures, and therefore will not affect thermodynamic equilibrium calculations, which presently must make the same assumption (that heats of mixing are negligible). The reasons for this unexpected sensitivity of the burning rate to ingredient heats of formation cannot be neatly isolated because it is a highly integrated effect, but it probably arises from a close competition between energy release by reactions and the locally dissipative processes of convection, conduction, and molecular diffusion.

Finally, I will express my belief that, while a full MD description of the gas phase will never be able to compete with the continuum description in terms of calculational efficiency and accuracy (for reasons discussed at the beginning of section 5), neither will a continuum description ultimately be able to compete with a discrete molecular description of the condensed-phase processes. It may be a long time before this promise is fulfilled, but if a complete description of propellant combustion is to be realized, there appears to be little choice but to pursue the MD approach tenaciously. In my discussions with molecular dynamicists, I have often observed an irrepressible optimism that the method can be made to work for phase changes, for subtle transport effects such as thermal diffusion, and even for reactive processes. However, examples given are usually for systems that are idealized in the extreme. To be applicable to a practical propellant burning-rate model, these simulations will have to be made to work for very general systems, even particularly difficult cases involving very large numbers of particles. Perhaps it is best that the dynamicists not fully understand the difficulties that await them!

6. Conclusions

In this work, I have made a reasoned attempt to predict the most promising course of future research aimed at predicting the burning rates of solid propellants from their ingredients. The last 15 years has seen the rise to dominance of models that treat the gas phase on the level of elementary reactions with full multicomponent transport. This explicit recognition of chemical specificity has been a necessary precursor to predictive capability. Energetic materials used as propellants are designed to produce gas pressure to accomplish work, and any model of burning rate must include descriptions of the condensed phase and the gasification mechanism. However, attempts to treat the condensed-phase and surface processes at the same level of rigor as the gas phase have been stymied by formidable difficulties in both experimental and theoretical approaches. It is possible that experiments may never be devised to provide the kind of accuracy

and detail that we have come to expect in the gas phase; at the least, it will probably be a very long time in coming. Despite this sobering possibility, we have shown that some degree of predictability may be possible using the semi-empirical approach embodied in the CYCLOPS code. At present, this predictability appears to be limited to members of well-studied classes of propellants, such as double-base and RDX/HMX/binder propellants. However, as continuing research encompasses ever wider classes of ingredients, generalizations for the semi-empirical aspects of the code may well enable wider applicability. For example, it has been suggested that a single pyrolysis law for most propellants might prove sufficient if the sensitivity of the burning rate to this law is low.

In my opinion, the greatest hope for treating the condensed-phase and surface processes in a full 3-phase, first-principles model lies with the developing field of reactive MD. Many obstacles, both known and unknown, will have to be overcome in treating condensed-phase reactions by this approach. It is not clear that reactive force fields with sufficient generality can be developed. It is not clear that methods for treating the many-body interactions can be developed with sufficient generality. However, there are ideas in the community about how to proceed; only time and effort will prove their value. It is worth remembering that burning rate is a highly integrated macroscopic consequence of almost unfathomably numerous microscopic processes. Because of this, the burning rate has often proved to be extraordinarily insensitive to the underlying processes. Thus, one may be justifiably hopeful that even an imperfect description of the detailed processes may lead to predictions of macroscopic phenomena that will provide insights and guidance of a practical nature in the development of new and optimized propellant formulations.

7. References

1. Miller, M. S.; Vanderhoff, J. A. *Burning Phenomena of Solid Propellants*; ARL-TR-2551; U.S. Army Research Laboratory: Aberdeen Proving Ground, MD, July 2001.

2. Adams, G. K. The Chemistry of Solid Propellant Combustion: Nitrate Ester or Double Base Systems. In *Mechanics and Chemistry of Solid Propellants;* Eringen, A.C., Liebowitz, H., Koh, S. L., Crowley, J. M., Eds.; Pergamon Press: Elmsford, NY, 1967.

3. Miller, M. S.; Anderson, W. R. Energetic-Material Combustion Modeling With Elementary Gas-Phase Reactions: A Practical Approach. In *Solid Propellant Combustion Chemistry, Combustion, and Motor Interior Ballistics*; Yang, V., Brill, T. B., Ren, W. Z., Eds.; Progress in Astronautics and Aeronautics Series; American Institute of Aeronautics and Astronautics: New York, 2000; Vol. 185, Chapter 2.12, pp 501–531.

4. Liau, Y.-C.; Yang, V. Analysis of RDX Monopropellant Combustion With Two-Phase Subsurface Reactions. *Journal of Propulsion and Power* **1995**, *11*, 729–739.

5. Davidson, J. E.; Beckstead, M. W. Improvements to Steady-State Combustion Modeling of Cyclotrimethylenetrinitramine. *Journal of Propulsion and Power* **1997**, *13*, 375–383.

6. Parr, R. G.; Crawford, B. L., Jr. A Physical Theory of Burning of Double-Base Rocket Propellants. I. *Journal of Physical and Colloid Chemistry* **1950**, *54*, 929–952.

7. Rice, O. K.; Ginell, R. The Theory of the Burning of Double-Base Rocket Powders. *Journal of Physical and Colloid Chemistry* **1950**, *54*, 885–917.

8. Streng, A. G. Combustion and Explosive Properties of Ozone. *Explosivstoffe* **1960**, *10*, 218–225.

9. Ben-Reuven, M.; Caveny, L. H. MAE Report 1455; Princeton University: Princeton, NJ, January 1980.

10. Miller, M. S. Three-Phase Combustion Modeling: Frozen Ozone, A Prototype System. In *Proceedings of the Materials Research Society Symposium: Decomposition, Combustion, and Detonation Chemistry of Energetic Materials*; Brill, T. B., Russell, T. P., Tao, W. C., Wardle, R. B., Eds.; Materials Research Society: Pittsburgh, PA, 1996; pp 169–180.

11. Sandri, R. On the Decomposition Flame of Liquid Ozone-Oxygen Mixtures in a Tube. *Combustion and Flame* **1958**, *2*, 348–352.

12. Miller, M. S. In Search of an Idealized Model of Homogeneous Solid Propellant Combustion. *Combustion and Flame* **1982**, *46*, 51–73.

13. Anderson, W. R.; Haga, S. W.; Nuzman, J. F.; Kotlar, A. J.; Anderson, R. J. U.S. Army Research Laboratory, Aberdeen Proving Ground, MD. PREAD Computer Code: A Versatile, Portable FORTRAN Computer Code for Interpreting the Complex Chemical Kinetics and Transport Properties of a Premixed, Laminar, Steady-State Flame, unpublished work, developed 1990–2002.

14. Anderson, R. J.; Nuzman, J. F.; Anderson, W. R.; Bitely, J. J. U.S. Army Research Laboratory, Aberdeen Proving Ground, MD. ChemPlot Computer Code: A Portable JAVA Computer Code for Rapid, On-line Visualization of Complex Chemical Kinetic Code Outputs, unpublished work, developed 1997–2002.

15. Anderson, R. J.; Anderson, W. R. U.S. Army Research Laboratory, Aberdeen Proving Ground, MD. ELEMAP: An Interactive, Portable, JAVA Computer Code for Rapid Visualization of Chemical Pathways Diagrams Related to Complex Chemical Kinetic Code Outputs, unpublished work, developed 1999–2002.

16. Hougen, O. A.; Watson, K. M. *Chemical Process Principles Charts*, 1st ed.; John Wiley & Sons: New York, 1946.

17. Fifer, R. A. Chemistry of Nitrate Ester and Nitramine Propellants. In *Fundamentals of Solid-Propellant Combustion*; K. K. Kuo, M. Summerfield, Eds.; Progress in Astronautics and Aeronautics Series; American Institute of Aeronautics and Astronautics: Reston, VA, 1984; Vol. 90.

18. Melius, C. F. Thermochemical Modeling: II. Application to Ignition and Combustion of Energetic Materials. In *Chemistry and Physics of Energetic Materials* **1990**; S. Bulusu, Ed.; NATO ASI Series, Kluwer Academic Publishers: Norwell, MA; Vol. 309; pp 51–78.

19. Prasad, K.; Yetter, R. A.; Smooke, M. D. An Eigenvalue Method for Computing the Burning Rates of RDX Propellant. *Combustion Science and Technology* **1997,** *124*, 35–82.

20. Zimmer-Galler, R. *AIAA Journal* **1968**, *6*, 2107–2110.

21. Glaskova, A. P. The Effects of Catalysis on the Combustion of Explosives. *Fizika Goreniya i Vzryva* **1974**, *10*, 323–334.

22. Miller, M. S. U.S. Army Research Laboratory, Aberdeen Proving Ground, MD. Unpublished data, 1985–1993.

23. Zenin, A. HMX and RDX: Combustion Mechanism and Influence on Modern Double-Base Propellant Combustion. *Journal of Propulsion and Power* **1995,** *11*, 752–758.

24. Ulas, A.; Lu, Y. C.; Kuo, K. K.; Freyman, T. In *Proceedings of the 32nd JANNAF Combustion Meeting*, Huntsville, AL, 23–27 October 1995; Chemical Propulsion Information Agency: Laurel, MD, 1995; CPIA Publication 631, Vol. I, pp 461–469.

25. Atwood, A. I.; Boggs, T. L.; Curran, P. O.; Parr, T. P.; Hanson-Parr, D. M. Burning Rate of Solid Propellant Ingredients, Part 1: Pressure and Initial Temperature Effects. *Journal of Propulsion and Power* **1999**, *15*, 740–747.

26. Homan, B. E.; Miller, M. S.; Vanderhoff, J. A. Absorption Diagnostics and Modeling Investigations of RDX Flame Structure. *Combustion and Flame* **2000**, *120*, 301–317.

27. Yetter, R. A.; Dryer, F. L.; Allen, M. T.; Gatto, J. L. Development of Gas-Phase Reaction Mechanisms for Nitramine Combustion. *Journal of Propulsion and Power* **1995,** *11*, 683–697.

28. Kee, R. J.; Grcar, J. F.; Smooke, M. D.; Miller, J. A. *A Fortran Program for Modeling Steady Laminar One-Dimensional Premixed Flames*; SAND85-8240; Sandia National Laboratories: Albuquerque, NM, December 1985; reprinted March 1991.

29. Miller, M. S.; Anderson, W. R. *CYCLOPS, A Breakthrough Code to Predict Solid-Propellant Burning Rates*; ARL-TR-2910; U.S. Army Research Laboratory: Aberdeen Proving Ground, MD, February 2003.

30. Miller, M. S.; Anderson, W. R. A Burning-Rate Predictor for Multi-Ingredient Propellants: Nitrate-Ester Propellants. *Journal of Propulsion and Power*, submitted for publication, 2002.

31. Zenin, A. A. *Study of Combustion Mechanism of Nitramine-Polymer Mixtures*; Final Technical Report; European Research Office of the U.S. Army: London, UK, November 1998; Contract No. N68171-97-M-5771.

32. Zenin, A. A. *Study of Combustion Mechanism of Nitramine-Polymer Mixtures*; Final Technical Report, European Research Office of the U.S. Army: London, UK, August 2000; Contract No. N68171-99-M-6238.

33. Zenin, A. A. *Study of Combustion Mechanism of New Polymer/Oxidizer Mixtures*; Final Technical Report, European Research Office of the U.S. Army: London, UK, May 2002; Contract No. N68171-01-M-5482.

34. Leider, H. R.; Seaton, D. L. *Nitrate Ester Decomposition and Degradation of Molecular Weight in Nitrocellulose From Thermal Decomposition of PBX-9404 Below 100 °C*; UCRL-52776; Lawrence Livermore National Laboratory: Livermore, CA, May 1979.

35. Todd, J.; Glasser, W. G. *NMR Spectroscopy of Nitrocellulose Samples;* In *Final Report on Cellulose and Cellulose Nitrate Characterization*; W. G. Glasser, A. G. Zink, Authors; Contract Report to AlliantTechSystems, Inc.: Radford, VA, February 1996; performed at Virginia Polytechnic Institute and State University, Blacksburg, VA, Section IV.

36. Bunte, S. W.; Miller, M. S. *Atomistic Simulations of the Physical Properties of Nitrate Esters*; ARL-TR-2496; U.S. Army Research Laboratory: Aberdeen Proving Ground, MD, May 2001.

37. Juhasz, A. A., Ed. *Round Robin Results of the Closed Bomb and Strand Burner*; CPIA Publication 361; Chemical Propulsion Information Agency: Laurel, MD, July 1982.

38. Atwood, A. I.; Price, C. F.; Curran, P. O.; Zwierzchowshi, N. G. Burning Rate, Radiant Ignition, and Global Kinetics of a Nitrocellulose Propellant. In *Proceedings of the 25th JANNAF Combustion Meeting*, Huntsville, AL, 24–28 October 1988; Chemical Propulsion Information Agency: Laurel, MD, 1988; CPIA Publication 498, Vol. I, pp 69–81.

39. Juhasz, A.; Bullock, C.; Homan, B.; Devynck, D. Micro Closed Bomb for Characterizing the Burning of Propellants at Gun Pressures. In *Proceedings of 36th JANNAF Combustion Subcommittee Meeting*, Cocoa Beach, FL, 18–21 October 1999; Chemical Propulsion Information Agency: Laurel, MD, 1999; CPIA Publication 691, Vol. I, pp 175–187.

40. Heller, C. A.; Gordon, A. S. Structure of the Gas Phase Combustion Region of a Solid Double Base Propellant; *Journal of Phys. Chem.* **1955**, *59*, 773.

41. Lengelle, G.; Bizot, A.; Duterque, J.; Trubert, J. F. Steady-State Burning of Homogeneous Propellants. In *Fundamentals of Solid Propellant Combustion;* Kuo, K., Summerfield, M., Eds.; Progress in Astronautics and Aeronautics Series; American Institute of Astronautics and Aeronautics: Reston, VA, 1984; Vol. 90.

42. Vanderhoff, J. A.; Anderson, W. R.; Kotlar, A. J. Dark Zone Modeling of Solid Propellant Flames. In *Proceedings of the 29th JANNAF Combustion Subcommittee Meeting*, Hampton, VA, 19–23 October 1992; Chemical Propulsion Information Agency: Laurel, MD, 1992; CPIA Publication 593, Vol. II, p 225.

43. Miller, M. S.; Anderson, W.R. *Prediction of Advanced-Nitramine-Propellant Burning Rates With the CYCLOPS Code*; ARL-MR-552; U.S. Army Research Laboratory: Aberdeen Proving Ground, MD, March 2003.

44. Reid, R. C.; Sherwood, T. K. *The Properties of Gases and Liquids*, 2nd ed.; McGraw-Hill: New York, 1966.

45. Reid, R. C.; Prausnitz, J. M.; Sherwood, T. K. *The Properties of Gases and Liquids*, 3rd ed.; McGraw-Hill: New York, 1977.

Appendix. Propellant Ingredients and Formulations

Propellant Ingredients:

ADN	ammonium dinitramide
AMMO	poly 3-azidomethyl-3-methyl oxetane
BAMO	poly 3,3-(bis)azidomethyl oxetane
CBIH	copolymer of butadiene and isoprene with hydroxyl terminated groups
CL20	2,4,6,8,10,12-hexanitrohexaazaisowurtzitane, rectangular crystal size $5 \times 3 \times 3$ μm
DEGDN	diethylene glycol dinitrate
GAP1U	glycidyl azide-polyurethane copolymer
GAP2	glycidyl azide polymer (molecular mass of 2000)
HMX	cyclotetramethylenetetranitramine
PU	polyurethane
PUNE	mixture of PU and NE
NC	nitrocellulose (cellulose nitrate)
NC1	cellulose mononitrate
NC2	cellulose dinitrate
NC3	cellulose trinitrate
NE	mixture of two nitroesters (dinitratdietileneglycole and dinitrattrietileneglicole)
NG	nitroglycerin (glycerin trinitrate)
RDX	cyclotrimethylenetrinitramine
THF	tetrahydrofuran

Nominal Propellant Formulations Assumed by CYCLOPS Code:

JA2	60% NC (13.1 %N), 25% DEGDN, 15% NG
M9	59.1% NC (13.25 %N), 40.9% NG
M10	100% NC (13.15 %N)

INTENTIONALLY LEFT BLANK.

2DEFENSE TECHNICAL
INFORMATION CENTER
DTIC OCA
8725 JOHN J KINGMAN RD
STE 0944
FT BELVOIR VA 22060-6218

1 COMMANDING GENERAL
US ARMY MATERIEL CMD
AMCRDA TF
5001 EISENHOWER AVE
ALEXANDRIA VA 22333-0001

1 INST FOR ADVNCD TCHNLGY
THE UNIV OF TEXAS AT AUSTIN
3925 W BRAKER LN STE 400
AUSTIN TX 78759-5316

1 US MILITARY ACADEMY
MATH SCI CTR EXCELLENCE
MADN MATH
THAYER HALL
WEST POINT NY 10996-1786

1 DIRECTOR
US ARMY RESEARCH LAB
AMSRL D
DR D SMITH
2800 POWDER MILL RD
ADELPHI MD 20783-1197

1 DIRECTOR
US ARMY RESEARCH LAB
AMSRL CS IS R
2800 POWDER MILL RD
ADELPHI MD 20783-1197

3 DIRECTOR
US ARMY RESEARCH LAB
AMSRL CI OK TL
2800 POWDER MILL RD
ADELPHI MD 20783-1197

3 DIRECTOR
US ARMY RESEARCH LAB
AMSRL CS IS T
2800 POWDER MILL RD
ADELPHI MD 20783-1197

ABERDEEN PROVING GROUND

2 DIR USARL
AMSRL CI LP (BLDG 305)
AMSRL CI OK TP (BLDG 4600)

NO. OF
COPIES ORGANIZATION

ABERDEEN PROVING GROUND

28 DIR USARL
AMSRL WM BD
W R ANDERSON
R A BEYER
A L BRANT
S W BUNTE
C F CHABALOWSKI
L M CHANG
T P COFFEE
J COLBURN
P J CONROY
R A FIFER
B E FORCH
B E HOMAN
S L HOWARD
P J KASTE
A J KOTLAR
C LEVERITT
K L MCNESBY
M MCQUAID
M S MILLER
A W MIZIOLEK
J B MORRIS
J A NEWBERRY
M J NUSCA
R A PESCE-RODRIGUEZ
G P REEVES
B M RICE
R C SAUSA
A W WILLIAMS

NO. OF COPIES	ORGANIZATION
1	M MILLER 1124 COWPENS AVE TOWSON MD 21286